CORA Cork Open Research Archive
Cartlann Taighde Oscailte Chorcaí

UCC Library and UCC researchers have made this item openly available. Please let us know how this has helped you. Thanks!

Title	IGF-1 receptor activity in the Golgi of migratory cancer cells depends on adhesion-dependent phosphorylation of Tyr1250 and Tyr1251
Author(s)	Rieger, Leonie; O'Shea, Sandra; Godsmark, Grant; Stanicka, Joanna; Kelly, Geraldine; O'Connor, Rosemary
Publication date	2020-05-26
Original citation	Rieger, L., O'Shea, S., Godsmark, G., Stanicka, J., Kelly, G. and O'Connor, R. (2020) 'IGF-1 receptor activity in the Golgi of migratory cancer cells depends on adhesion-dependent phosphorylation of Tyr1250 and Tyr1251', Science Signaling, 13(633), eaba3176. doi: 10.1126/scisignal.aba3176
Type of publication	Article (peer-reviewed)
Link to publisher's version	http://dx.doi.org/10.1126/scisignal.aba3176 Access to the full text of the published version may require a subscription.
Rights	**© 2020, the Authors. Published under license by the American Association for the Advancement of Science. This is the author's version of the work. It is posted here by permission of the AAAS for personal use, not for redistribution. The definitive version was published in Science Signaling 13(633) on 26 May 2020, doi: 10.1126/scisignal.aba3176**
Item downloaded from	http://hdl.handle.net/10468/10125

Downloaded on 2020-06-06T01:30:34Z

UCC University College Cork, Ireland
Coláiste na hOllscoile Corcaigh

IGF-1 receptor activity in the Golgi of migratory cancer cells depends on adhesion-dependent phosphorylation of tyrosines 1250 and 1251

Leonie Rieger[1], Sandra O'Shea[1], Grant Godsmark[1], Joanna Stanicka[1], Geraldine Kelly[1] and Rosemary O'Connor[1]*

[1] Cell Biology Laboratory, School of Biochemistry and Cell Biology, BioSciences Institute, University College Cork, Cork, Ireland

*Corresponding author. Email: r.oconnor@ucc.ie

Abstract

Although insulin-like growth factor (IGF-1) signaling promotes tumor growth and cancer progression, therapies that target the IGF-1 receptor (IGF-1R) have shown poor clinical efficacy. To addresses IGF-1R activity in cancer cells and how it differs from that of the closely related insulin receptor (IR), we focused on two tyrosines in the IGF-1R C-terminal tail that are not present in the IR and are essential for IGF-1–mediated cancer cell survival, migration, and tumorigenic growth. We found that Tyr^{1250} and Tyr^{1251} ($Tyr^{1250/1251}$) were autophosphorylated in a cell adhesion–dependent manner. To investigate the consequences of this phosphorylation, we generated phosphomimetic Y1250E/Y1251E (EE) and non-phosphorylatable Y1250/Y1251F (FF) mutant forms of IGF-1R. Although fully competent in kinase activity and signaling, the EE mutant was more rapidly internalized and degraded than either the wild-type or FF receptor. IGF-1 promoted accumulation of wild-type and EE IGF-1R within the Golgi apparatus, whereas the FF mutant remained at the plasma membrane. Golgi-associated IGF-1R signaling was a feature of migratory cancer cells, and Golgi disruption impaired IGF-1–induced signaling and cell migration. Upon the formation of new cell adhesions, IGF-1R transiently re-localized to the plasma membrane from the Golgi. Thus, phosphorylation at $Tyr^{1250/1251}$ promoted IGF-1R

translocation to and signaling from the Golgi to support an aggressive cancer phenotype. This could contribute to the poor clinical efficacy of antibodies that target IGF-1R on the cell surface and also distinguish IGF-1R from IR signaling.

Introduction

The receptor-like tyrosine kinase (RTK) insulin-like growth factor–1 receptor (IGF-1R) and its ligands (IGF-1 and IGF-2) are widely present throughout different cell and tissue types and play essential roles in cell, organ, and organismal growth (*1, 2*). The IGF system is also linked to cancer risk, tumorigenesis, tumor growth and survival, and to promoting cell migration in both normal and transformed cells (*3-6*). Many pre-clinical studies have shown a clear effect of IGF-1R suppression or inhibition on limiting tumorigenesis, tumor growth and metastatic potential (*3, 4, 6*). However, this has not been replicated in large-scale clinical trials, wherein IGF-1R blocking antibodies and kinase inhibitors show an overall poor efficacy (*3, 4*). There are no predictive biomarkers for IGF-1R activity, and there is limited understanding of the cellular signaling events that promote resistance to or evasion of IGF-1R inhibitors.

Although IGF-1 signaling in cancer cells has been extensively studied, it is still poorly understood how IGF-1R expression, abundance, and signaling output are influenced by oncogenic and adhesion signals in different cancers. Amounts of cell surface IGF-1R may not predict responses to ligand stimulation in terms of downstream signaling output, and this is apparently influenced by the cancer cell phenotype, such as migratory versus non migratory (*7*). We and others previously demonstrated that adhesion signals enhance IGF-1R activation and signaling, and that integrin-mediated signaling is essential for IGF-1 to promote cancer cell proliferation and migration (reviewed in (*8*)). Moreover, the association of IGF-1R with E-

cadherin and with discoidin domain receptors (DDRs), which are receptor tyrosine kinases activated by binding to collagen, can control receptor stability and signaling output (*9-11*).

Cooperation between integrin β1 and IGF-1R signaling involves an adhesion-dependent signaling complex composed of scaffolding proteins, focal adhesion kinase (FAK), and phosphatases that ultimately leads to activation of mitogen-activated protein kinase (MAPK) pathways (*12-15*). Mutation of two tyrosines (Tyr^{1250} and Tyr^{1251}) in the C-terminal tail of IGF-1R is sufficient to abrogate the receptor's function in facilitating cellular transformation, cell survival, and migration (*16-18*). These tyrosine residues were also found to be essential for integrating IGF-1R and adhesion signaling (*14*). However, these tyrosines are not present in the human insulin receptor (IR), which has an almost identical kinase domain to the IGF-1R but shares less than 50% homology with the C-terminal tail. We previously hypothesized that the function of these tyrosines may distinguish IGF-1R and IR actions in cell growth and cancer (*14, 17, 19*). However, despite the clear loss of IGF-1R function observed upon mutation of Tyr^{1250} and Tyr^{1251} ($Tyr^{1250/1251}$) to phenylanines (Y1250F/Y1251F), and in silico predictions for phosphorylation in cells (*14, 16-21*), evidence for actual phosphorylation in vivo has remained elusive, as has knowledge of how this phospho-site functions. This has hindered efforts to understand how these IGF-1R tyrosines facilitate tumourigenesis or how this site may distinguish IGF-1R and IR signaling.

In this study, using mass spectroscopy and phospho-specific antibodies, we established that the IGF-1R was basally autophosphorylated on $Tyr^{1250/1251}$ in cells, and this depended on IGF-1 and adhesion signaling. We determined the functions of $Tyr^{1250/1251}$ phosphorylation by using a phosphomimetic mutant (Y1250E/Y1251E, referred to as the EE mutant) form of IGF-1R, which was more rapidly internalized and less stable than the wild-type IGF-1R or the

Y1250F/Y1251F (FF) mutant. Upon IGF-1 stimulation, both the wild-type and the EE mutant IGF-1R rapidly accumulated within the Golgi apparatus, whereas the FF mutant was retained on the plasma membrane. IGF-1R localization in the Golgi-apparatus was associated with migratory potential, and an intact Golgi apparatus was required for IGF-1R signaling in migrating cells. Overall, the data indicate that $Tyr^{1250/1251}$ phosphorylation drives translocation of IGF-1R to the Golgi, where it contributes to a migratory phenotype. These results distinguish IGF-1R and IR function, and may also explain the inefficacy of targeting cell surface IGF-1R with monoclonal antibodies in several cancers.

Results

Phosphorylation of IGF-1R on Tyr^{1250} and Tyr^{1251} occurs in cells

First, to address the question whether the $Tyr^{1250/1251}$ site becomes phosphorylated in cells, we used mass spectroscopy and phosphopeptide analysis of IGF-1R immunoprecipitated from mouse embryonic fibroblasts derived from IGF-1R knockout mice (R- cells) transiently expressing the receptor and either serum-starved or stimulated with IGF-1. The isolation of IGF-1R phosphopeptides including $Tyr^{1250/1251}$ was less efficient than isolation of other phosphopeptides from the receptor, which we attributed to the fact that these tyrosines reside within a sequence (SFYYS) that also includes phosphorylated serines (*20, 22*), and would thus be highly charged and difficult to capture. Following peptide extraction and mass spectrometry analysis, a series of phosphopeptides was identified (ion score >19) containing tyrosines that are known to be phosphorylated in response to IGF-1, including Tyr^{950} and the kinase activation site tyrosines Tyr^{1131}, Tyr^{1135}, and Tyr^{1136} (Fig. 1A). In addition, phosphopeptides were captured

from both serum-starved and IGF-1–stimulated cells with phosphorylation on the Tyr^{1250} site, with a higher score indicating IGF-1–induced phosphorylation (Fig. 1A).

We next employed an antibody specific for the phosphorylated $Tyr^{1250/1251}$ site to further assess $Tyr^{1250/1251}$ phosphorylation over time in response to either serum starvation or IGF-1. In phosphopeptide arrays, an antibody known to recognize phosphorylated Tyr^{1250} also detected peptides containing either the single phosphorylated site or the doubly phosphorylated site (fig. S1, A and B), and we therefore concluded that this antibody reacts with the $Tyr^{1250/1251}$ phosphosite. We next compared the profile of IGF-1–stimulated phosphorylation of the $Tyr^{1250/1251}$ phosphosite with the IGF-1R autophosphorylation sites Tyr^{950}, Tyr^{1131}, and $Tyr^{1135/1136}$. This analysis demonstrated that basal amounts of Tyr^{950}, Tyr^{1130}, and Tyr $^{1135/1136}$ phosphorylation were low and then rapidly induced by IGF-1 at 1-5 min. In contrast, basal phosphorylation of $Tyr^{1250/1251}$ was evident in serum-starved cells, and IGF-1–induced phosphorylation at this site accumulated more slowly than it did at the other sites (Fig. 1B). This result is consistent with the mass spectrometry analysis indicating phosphorylation in serum-starved cells (Fig. 1A).

Although IGF-1 displays greater affinity for IGF-1R than for IR, and insulin displays greater affinity for IR than for IGF-1R, each can activate the other receptor when the ligand concentration is high. Therefore, we investigated whether $Tyr^{1250/1251}$ phosphorylation was influenced by ligand concentration in serum-starved R- cells expressing wild-type (WT) IGF-1R stimulated with either 1, 10, 50, or 100 ng/ml IGF-1. From this we observed that $Tyr^{1250/1251}$ phosphorylation was induced in a dose-responsive manner with highest amounts of phosphorylation reached at 50 ng/mL (Fig. 1C). Insulin did not induce phosphorylation on $Tyr^{1250/1251}$ even at 100 ng/mL, although it modestly induced phosphorylation of the kinase AKT,

which is known to mediate activation of the mTOR pathway, metabolism, growth and survival, but not phosphorylation of extracellular signal–regulated kinase (ERK), known to promote mitogenic, differentiation and migratory signals, at this concentration (Fig. 1D). IGF-2 also induced $Tyr^{1250/1251}$ phosphorylation (Fig. 1D). We also observed phosphorylation on $Tyr^{1250/1251}$ of endogenous IGF-1R in the cancer cell lines MDA-MB-231, Cal-51, HS-578T, and DU-145 (Fig. 1E). Again, $Tyr^{1250/1251}$ phosphorylation was observed in serum-starved cells, and this increased upon IGF-1 stimulation (Fig. 1E). Together, these data demonstrate that $Tyr^{1250/1251}$ phosphorylation was present in cells at low basal amounts and was induced by IGF-1 in a concentration- and time-dependent manner.

Adhesion signals and IGF-1R kinase activity are required for $Tyr^{1250/1251}$ phosphorylation

Because IGF-1 enhanced phosphorylation of IGR-1R at $Tyr^{1250/1251}$ and this phosphorylation event had not previously been demonstrated in cells, we next investigated whether it was a *bona fide* autophosphorylation site in IGF-1R. The first approach was to determine whether $Tyr^{1250/1251}$ phosphorylation could be induced in the presence of an inhibitor of IGF-1R kinase activity. In serum-starved cells $Tyr^{1250/1251}$ phosphorylation was not affected by the IGF-1R kinase inhibitor BMS754807 (Fig. 2A). However, IGF-1–mediated enhancement of $Tyr^{1250/1251}$ phosphorylation was abolished by the kinase inhibitor, indicating that IGF-1–induced phosphorylation of $Tyr^{1250/1251}$ was likely a result of autophosphorylation. To further test autophosphorylation, we assessed autophosphorylation of WT IGF-1R and a kinase-inactive form of IGF-1R (K1003R, an ATP-binding site mutant, referred to henceforth as KR), in the absence or presence of exogenously added ATP to stimulate kinase activity. Although phosphorylation on $Tyr^{1250/1251}$ was detectable on both the WT and KR receptors, this was increased by exogenous ATP on the

WT but not on the KR receptor (Fig. 2B). This indicates that IGF-1R kinase activity was required for phosphorylation on $Tyr^{1250/1251}$. The observation that phosphorylation was evident with the KR mutant and with WT IGF-1R in serum-starved cells also suggests that other cellular kinases may phosphorylate $Tyr^{1250/1251}$.

Previous studies have shown that the $Tyr^{1250/1251}$ site is required for cooperative IGF-1R and adhesion signaling (*14*) and that IGF-1R kinase activity is influenced by adhesion signaling and adhesion-associated kinases (*23, 24*). Therefore, we asked whether adhesion-activated kinases (FER, FAK and Src) contributed to $Tyr^{1250/1251}$ phosphorylation. To test this we used Cal-51 breast cancer cells, in which IGF-1 and adhesion signaling are active (*10, 25*), and measured IGF-1–induced phosphorylation at the $Tyr^{1250/1251}$ site and at the $Tyr^{1135/1136}$ site, which is required for full kinase activation, in the presence of either the IGF-1R kinase inhibitor BMS-754807, a FER kinase inhibitor (AP-26113), a FAK kinase inhibitor (PF-573228), or a Src kinase inhibitor (PP2) (Fig. 2C). We observed that IGF-1–induced phosphorylation on both sites was decreased by BMS, AP-26113, and PF-573228 but not by PP2 (Fig. 2C). Thus, inhibition of IGF-1R, FER or FAK kinase activity suppressed IGF-1R autophosphorylation and full kinase activation. A requirement for adhesion signaling in full IGF-1R autophosphorylation was also observed with cells that were detached from the substratum. IGF-1–stimulated phosphorylation of the Tyr^{950}, Tyr^{1131}, $Tyr^{1135/1136}$, and $Tyr^{1250/1251}$ sites was reduced by detachment of R- cells expressing WT IGF-1R, as well as by detachment of Cal-51 and DU-145 cancer cells (Fig. 2, D and E). IGF-1–induced activation of AKT and ERK was also reduced in detached cells compared to adherent cells (Fig. 2, D and E). We conclude that both IGF-1R and adhesion signaling were essential for maximal phosphorylation of the IGF-1R on $Tyr^{1250/1251}$ and that cell adhesion enhanced overall IGF-1R autophosphorylation and activation.

A Tyr$^{1250/1251}$ phosphomimetic mutant IGF-1R is fully active but rapidly turned over

The next question to be addressed was how phosphorylation on the Tyr$^{1250/1251}$ site contributed to IGF-1R function and signaling. To address this, we generated a phosphomimetic for this site, a mutant IGF-1R with tyrosines Tyr$^{1250/1251}$ substituted by negatively charged glutamic acids, the EE mutant. When transiently transfected into either R- cells or three different cancer cell lines (MCF-7, MDA-MB-231, DU-145) in which the IGF-1R was knocked out by CRISPR technology, the EE mutant was consistently expressed at significantly lower levels than either the WT or FF IGF-1R (Fig. 3A). A similar pattern of lower receptor protein abundance was observed in R- cells stably expressing EE IGF-1R (fig. S2A), although mRNA expression across the transfected WT, FF, and EE constructs was similar (fig. S2B). Single mutation of either Tyr^{1250} or Tyr^{1251} to glutamic acid was also sufficient to impair receptor protein abundance compared to WT IGF-1R (fig. S2C).

Although present in lower amounts in cells, the EE mutant was observed to be functional and to mediate IGF-1–stimulated kinase activation and downstream signaling. Cells expressing either WT or EE IGF-1R exhibited similar IGF-1–stimulated AKT and ERK activation (Fig. 3B). The FF mutant exhibited lower IGF-1R and ERK activity than WT IGF-1R (Fig. 3B), which is consistent with previous studies (*19*). Transient overexpression of WT, FF, or EE IGF-1R in MDA-MB-231 IGF-1R knockout cells (MDA-KO) also demonstrated that the activation of EE IGF-1R was comparable to that of WT IGF-1R, whereas it was higher than that of FF IGF-1R (Fig. 3C). In vitro kinase assays were used to compare the IGF-1R kinase activity of the EE mutant with WT IGF-1R and the FF mutant. In vitro EE IGF-1R kinase activity was similar to

that of WT IGF-1R, whereas FF IGF-1R kinase activity was lower than that of WT IGF-1R (Fig. 3D), as also previously reported (*17*).

The lower cellular abundance of the EE mutant compared to WT IGF-1R and the FF mutant suggested that $Tyr^{1250/1251}$ phosphorylation influenced the translation or stability of the IGF-1R protein. We first ruled out the possibility that low EE protein was due to impaired protein synthesis by using cycloheximide (CHX) to transiently suppress protein synthesis, and then assessing the amount of newly synthesized protein over time. In these experiments it was clear that similar amounts of WT IGF-1R and mutant IGF-1Rs were restored following CHX exposure (Fig. 4A), thereby indicating similar amounts of synthesis. We next tested whether inhibition of proteasomal or lysosomal activity could restore EE IGF-1R protein in cells. The IGF-1R protein is synthesized as a pro-receptor that is processed to yield an extracellular α chain and intracellular β chain. The functional receptor is a homo-dimer of two α chains and two β chains that are joined by disulphide bonds. Inhibition of proteasomal activity with MG-132 for 6hr restored the EE β-chain to protein abundances that were similar to those of WT IGF-1R and FF IGF-1R in control cells, and the abundance of the pro form of the receptor was also recovered (Fig. 4B). Lysosomal inhibition with E64D+Leupeptin or Chloroquine did not affect EE protein abundance (Fig. 4C), indicating that the EE mutant was not more susceptible to lysosomal degradation than WT.

We also investigated whether stimulation of R- cells with high or low concentrations of IGF-1 influenced the degradation of the EE and WT IGF-1R compared to the FF IGF-1R. This demonstrated that IGF-1 stimulation at either high or low IGF-1 concentrations resulted in a similar reduction in amounts of the WT and EE receptors at 6 and 12 hours, whereas the abundance of the FF receptor was not significantly reduced after 6 hours and was comparable to

its abundance in unstimulated cells (Fig. 4D). Thus, the FF mutant was protected from degradation. Together, these results demonstrate that the IGF-1R EE mutant was kinase-active and responsive to IGF-1 but was less stable than WT IGF-1R. The data suggest that $Tyr^{1250/1251}$ phosphorylation accelerated IGF-1R protein turnover.

$Tyr^{1250/1251}$ phosphorylation promotes IGF-1R translocation to the Golgi apparatus

The IGF-1R EE mutant was highly active in signaling even with low amounts of protein in the cells, so we next investigated its subcellular location and compared IGF-1–stimulated internalization and trafficking of the EE receptor with that of the WT and FF receptors. Although, as expected, the WT receptor was mainly located on the cell membrane in serum-deprived cells, we observed that a pool of IGF-1R was located at the perinuclear region in these cells (Fig. 5A). In IGF-1–stimulated cells, both WT and EE receptors were visible in large intracellular vesicles. Over time these vesicles appeared to accumulate at the perinuclear region and were less evident at the plasma membrane (Fig. 5A). These IGF-1R–containing vesicles were overall less evident in cells expressing the FF mutant receptor, in which the receptor was predominantly located at the plasma membrane (Fig. 5A). The relative translocation patterns of IGF-1R WT and EE in cells were illustrated by showing the intensity in IGF-1R fluorescence signal along a line that was drawn diagonally from cell membrane to cell membrane through the nucleus (Fig. 5B). Without IGF-1, cells expressing the EE mutant exhibited a clear peak in IGF-1R fluorescence signal close to the nucleus. This peak was less prominent in cells expressing WT IGF-1R and was not visible in cells expressing FF IGF-1R. Over time cells expressing either WT or EE displayed a shift in IGF-1R fluorescence signal towards the nucleus and a reduction in signal intensity near the plasma membrane.

Receptor internalization was also assessed using in-cell Western assays to quantify the ratio of IGF-1R present at the plasma membrane relative to total amount of the receptor in cells that were stimulated with IGF-1. Whereas the amounts of the receptor at the cell surface declined in response to IGF-1 in cells expressing either the WT or EE receptors, the cell surface amounts of FF receptors were not altered (Fig. 5C). To test whether WT and EE IGF-1Rs were being actively internalized into vesicles, we used an antibody that recognizes the α chain of IGF-1R (IRα) and is known to induce IGF-1R internalization (*3*). R- cells expressing the WT, FF, or EE IGF-1R were serum-starved for 4 hr and cultured with the IRα antibody for 30 min either at 37˚C (Fig. 5D) or on ice (fig. S3A) followed by staining with an antibody detecting the β chain of IGF-1R and immunofluorescence analysis for co-localization (Fig. 5D, fig. S3B). The IRα-specific antibody was internalized in vesicles after 30 min in cells expressing the WT or EE IGF-1R, whereas co-localization of IRα with the β-chain was observed at the plasma membrane in cells expressing the FF mutant. We conclude that activated WT and EE IGF-1Rs were rapidly internalized into intracellular vesicles that accumulated at the perinuclear region over time. The observation that the FF mutant neither accumulated within vesicles nor underwent post-endocytotic trafficking suggests that phosphorylation on $Tyr^{1250/1251}$ was required for internalization and accumulation of IGF-1R at the perinuclear region.

Post-endocytic trafficking of surface receptors and proteins to the Golgi apparatus has been described as retrograde trafficking and a process that may be important for cell signaling (*26, 27*). We therefore further investigated IGF-1R co-localization with the Golgi marker GM130 in cells expressing WT, FF, or EE IGF-1R. Over time, the WT and EE IGF-1Rs co-localized with GM130 at the *cis*-Golgi compartment (Fig. 6A). Co-localization of IGF-1R with a biotinylated form of the lectin VVA, which labels N-acetylgalactosamine and is a marker for

both *trans*- and *cis*-Golgi, was also evident (Fig. 6B). The EE mutant was also observed at the Golgi apparatus in serum-starved cells, suggesting that phosphorylation on $Tyr^{1250/1251}$ was sufficient for translocation to the Golgi. To further test whether WT and EE IGF-1Rs were present in the Golgi apparatus, we used Brefeldin A (BFA) to induce *cis*-Golgi fragmentation (*28*) in R- cells expressing the WT, EE, or FF receptor. Fragmentation of the *cis*-Golgi resulted in lower amounts of WT and EE receptors (Fig. 6C), whereas BFA did not affect the FF mutant receptor. Taken together, these results indicate that IGF-1-induced internalization and accumulation of the IGF-1R in the Golgi apparatus required phosphorylation on $Tyr^{1250/1251}$.

$Tyr^{1250/1251}$ phosphorylation and adhesion signals promote IGF-1R presence in and signaling from the Golgi

The $Tyr^{1250/1251}$ site is required to support a transformed phenotype, cancer cell survival, cell migration, tumor growth, and metastasis in vivo (*3, 18, 29*). Because Golgi-derived signaling is implicated in cell migration (*30*), we hypothesized that $Tyr^{1250/1251}$ phosphorylation and IGF-1R Golgi localization may be a feature of migratory cancer cells. To test this, we compared IGF-1R localization in non-migratory MCF-7 cancer cells to that in migratory MDA-MB-231 and HS-578T cells, both of which also exhibited relatively high IGF-1R $Tyr^{1250/1251}$ phosphorylation (Fig. 1E). Whereas the IGF-1R was evident at sites of focal adhesion (FA) in MCF-7 cells, it was also clearly located within the Golgi apparatus in MDA-MB-231 and HS-578T cells (Fig. 7A). IGF-1R abundance was reduced by the Golgi disruptor BFA in MDA-MB-231 and HS-578T cells, but not in MCF-7 cells (Fig. 7B). Furthermore, although disruption of the Golgi with BFA did not alter the distribution of the IGF-1R at the plasma membrane in MCF-7 cells, BFA caused dispersal of the IGF-1R from the Golgi apparatus in MDA-MB-231 and HS-578T cells (Fig. 7C).

In these cells IGF-1R staining remained visible at the leading edge within lamellipodia. IGF-1–induced phosphorylation on $Tyr^{1250/1251}$ was detectable in both MCF-7 and HS-578T cells, but basal amounts of SHC [Src homology 2 (SH2) domain–containing] phosphorylation and IGF-1–induced SHC phosphorylation were impaired by BFA in HS-578T cells, but not in MCF-7 cells (Fig. 7D).

Because IGF-1R was observed at the lamellipodia of cells even when the Golgi was disrupted (Fig. 7C) and $Tyr^{1250/1251}$ phosphorylation required adhesion signaling (Fig. 2C-E), we next investigated whether cell adhesion controlled IGF-1R localization at the plasma membrane or Golgi in MCF-7 and HS-578T cells. IGF-1R location and phosphorylation on $Tyr^{1250/1251}$ was monitored over time in response to the formation of nascent FA contacts in cells that were allowed to attach to fibronectin-coated plates and coverslips. Immunofluorescence showed that the IGF-1R was present at the plasma membrane in both cell types at 15 min after cell seeding (Fig. 8A). At this time phosphorylation on $Tyr^{1250/1251}$ was low (Fig. 8B). In MCF-7 cells the IGF-1R was observed in FAs at 30 min after cell seeding, and it remained there for up to 60 min (Fig. 8A). In HS-578T cells, most of the IGF-1R had moved from the plasma membrane to the Golgi at 30 min and was exclusively Golgi-localized by 60 min (Fig. 8A). In MCF-7 cells phosphorylation on $Tyr^{1250/1251}$ remained low over time after cell adhesion, whereas in HS-578T cells $Tyr^{1250/1251}$ phosphorylation increased over time after adhesion (Fig. 8B). These observations indicate that the IGF-1R was rapidly recruited to nascent FAs in HS-578T cells and that IGF-1R and adhesion-dependent $Tyr^{1250/1251}$ phosphorylation promoted subsequent translocation of the receptor to the Golgi.

Directed migration of epithelial cells requires the formation of leading edge protrusion and adhesion to the extracellular matrix (ECM), which involves the formation of new FAs (*30*).

We therefore investigated whether the IGF-1R was recruited to FAs in migrating cells. At 6 hr after wounding a HS-578T cell monolayer, large FAs were visible at the leading edge of the migrating cells (Fig. 8C). In agreement with our earlier observations of IGF-1R at sites of adhesion in both migratory and nonmigratory cells (Fig. 7A), immunofluorescence analysis showed that the IGF-1R was clearly located within the protrusions of moving cells (Fig. 8C). In these cell cultures it was also clear that the IGF-1R was predominantly located in the Golgi apparatus within cells that were part of the high confluency monolayer. BFA abolished IGF-1–stimulated HS-578T cell migration (Fig. 8D), indicating that the Golgi apparatus is essential for IGF-1-promoted cell migration.

To better understand what promoted IGF-1R localization to the Golgi, we further assessed IGF-1R localization in MCF-7 and HS-578T cells that were cultured to either sub-confluence, which allows for cell migration and cell-matrix contacts, or high confluence, which favors cell-cell adhesion. We observed that when cell-cell adherence was high in MCF-7 cells, the IGF-1R was located at the plasma membrane sites of cell-cell adhesion as previously described (*9*), whereas it was located at sites of focal cell adhesion in sub-confluent cultures (Fig. 8E). In these MCF-7 cultures, basal phosphorylation on $Tyr^{1250/1251}$ was present, and IGF-1–induced phosphorylation of SHC was evident (Fig. 8F). In contrast, in sub-confluent HS-578T cells, the IGF-1R was located at the leading edge and in the Golgi with significant IGF-1–induced phosphorylation of $Tyr^{1250/1251}$ evident, whereas in confluent cells the IGF-1R was predominantly located in the Golgi (Fig. 8E), where constitutive $Tyr^{1250/1251}$ phosphorylation was evident (Fig. 8, E and F). HS-578T cells growing under high-confluency conditions exhibited little IGF-1–stimulated SHC phosphorylation (Fig. 8F). However, induction of phosphorylation on $Tyr^{1135/1136}$ and activation of AKT and ERK was present, confirming that the IGF-1R was

active within the Golgi in these cells. Taken together, these data indicate that phosphorylation on $Tyr^{1250/1251}$ promoted the accumulation of IGF-1R in the Golgi. Within the Golgi, the IGF-1R was active and induced downstream signaling. On the other hand, cell-ECM adhesion signals during cell migration enhanced IGF-1–induced phosphorylation on $Tyr^{1250/1251}$, resulting in the IGF-1R being located both in the Golgi and at the leading edge of migrating cells.

Discussion

Although IGF-1 signaling has a well-described function in facilitating tumorigenesis and promoting tumor growth, it is unresolved why the abundance of IGF-1R does not correlate with its activity in cancer cells and why IGF-1R–targeting drugs have been largely ineffective. Our findings here (summarized in the model in Fig. 9) explain a previously hidden activity of the IGF-1R in promoting an aggressive cancer phenotype and evading therapy. Adhesion-dependent phosphorylation of the IGF-1R on $Tyr^{1250/1251}$ promoted receptor translocation from the plasma membrane to the Golgi, whence it elicited signaling and was available for transport to and from new FA sites in migrating cells. Ligand- and adhesion-stimulated $Tyr^{1250/1251}$ phosphorylation and receptor internalization also accelerated the turnover of the receptor.

Previous studies have reported that IGF-1R activity and signaling can be modulated by cell adhesion signals (reviewed in (*8*)) and directly by adhesion-associated kinases including FAK, Src, and FER (*23, 24, 31-33*). The presence of $Tyr^{1250/1251}$ is necessary for the integration of IGF-1R and integrin β1 signaling mediated by their co-recruitment into a scaffolding complex containing RACK-1, SHC, and other mediators that stimulate MAPK signaling (*12, 14*). Loss of this interaction with mutation of the tyrosines to phenylalanine results in impaired IGF-1–induced cell migration and tumor growth in vivo (*14, 18*). Our observations here, specifically

that the phosphomimetic EE mutant (for $Tyr^{1250/1251}$ phosphorylation) was more rapidly internalized and trafficked from the Golgi apparatus to the leading edge of migrating cells, indicate that phosphorylation on this site is necessary for cooperation with adhesion signaling. IGF-1 also stimulates the internalization of WT IGF-1R to the Golgi, demonstrating that this is an intrinsic component of IGF-1R signaling when it is phosphorylated on these residues. In migrating cells, the removal of IGF-1R from FA points induced by phosphorylation on $Tyr^{1250/1251}$ may facilitate the disassembly of FAs to promote the migration of cells, and may also explain the impaired migratory capacity of cells expressing the FF mutant, wherein the IGF-1R is retained at the plasma membrane.

It is well documented that the outcome of RTK activation and signaling can vary depending on receptor location (*34-36*). Compartmentalization of RTK signaling may facilitate the recruitment of different effector proteins that might be dictated by a specific cell phenotype. Emerging evidence suggests an important role for the Golgi in oncogenic RTK signaling (*37-39*). Overexpressed or mutated forms of the RTK MET cause ligand-independent activation and signaling from MET, including the phosphorylation of the RTK human epidermal growth factor receptor 3 (HER3, also known as ERBB3), in the Golgi (*37*). Similarly, mutated forms of the RTK KIT are retained in the Golgi where they are active and induce downstream signaling (*38, 40-42*). The RTKs vascular endothelial growth factor receptor 2 (VEGFR2), fibroblast growth factor receptor (FGFR2) and epidermal growth factor receptor (EGFR, also called HER1 and ERBB1) are also reported to be located at and induce signaling from the Golgi (*27, 35, 43*). Our findings with the IGF-1R add important knowledge to the understanding of Golgi-derived RTK signaling because we demonstrate that trafficking of this RTK to the Golgi apparatus is promoted by a specific adhesion- and ligand-dependent phosphorylation on $Tyr^{1250/1251}$. In migrating cells

the IGF-1R was located at the leading edge of nascent FAs and was subsequently rapidly trafficked back to the Golgi. This suggests that a pool of IGF-1R phosphorylated at $Tyr^{1250/1251}$ is stored in the Golgi for signaling and fast trafficking back to the membrane in migrating cells. Indeed, a similar trafficking route is proposed for Golgi membrane protein 1 (GOLM)–mediated trafficking of ligand-activated EGFR in hepatocellular carcinoma (*27*).

We have not however established if the IGF-1R is a cargo protein, if it might participate in regulating the secretion of proteins from the Golgi, or what controls its trafficking out of the Golgi. Phosphorylation on $Tyr^{1250/1251}$ was low when the IGF-1R was recruited to the membrane, which suggests that phosphatases may facilitate the dephosphorylation of $Tyr^{1250/1251}$, leading to the release of IGF-1R from its Golgi location. Once located at points of nascent FAs, the IGF-1R may promote the recruitment of other interaction partners and proteins leading to the stabilization of FAs. It is likely that the IGF-1R is subsequently removed from FAs following phosphorylation on $Tyr^{1250/1251}$. An alternative possibility is that the IGF-1R traffics to the Golgi compartment as part of a multi-protein complex that is stored there for signaling.

Golgi-derived oncogenic signaling may be especially active in cell migration (*30*). Here we observed that fragmentation of the Golgi impaired cell migration in the presence of IGF-1. This was associated with impaired SHC phosphorylation in migratory HS-578T cells but not in non-migratory MCF-7 cells. This is consistent with a previously described requirement for an intact Golgi apparatus in activating the RAS pathway and ERK signaling to establish cell polarity in migrating cells (*30*). The observation that impaired SHC phosphorylation was not observed in non-migratory cells suggests that different signaling outcomes can be dictated by the same receptor depending on its location and on the cell phenotype as previously suggested (*7*). Our data suggest that distinct cell adhesion signals have an essential function in determining

IGF-1R autophosphorylation and location. Mesenchymal cancer cells exhibiting high migratory capacity and aggressiveness are often deficient in E-cadherin, which interacts with the IGF-1R and may retain it at cell-cell junctions in, for example, MCF-7 cells (*9*). Loss of E-cadherin would therefore be likely to alter IGF-1R localization and potentially facilitate interactions with integrins.

Activated intracellular and nuclear IGF-1R have previously been linked to an aggressive cancer phenotype. Intracellular IGF-1R is more abundant in malignant than in benign epithelium in samples from prostate cancer patients (*44*), and nuclear IGF-1R has been proposed to facilitate breast and prostate cancer (*45, 46*). Moreover, although abundance of the IGF-1R itself is not associated with survival in breast cancer patients, high amounts of IGF-1R phosphorylation are linked to poor outcomes (*47*). Our finding of Golgi-derived IGF-1R signaling offers a mechanistic explanation for these effects, because although the EE IGF-1R was present in lower amounts in cells, it retained high activity.

In summary, phosphorylation-specific trafficking of the IGF-1R to the Golgi and the association of this with aggressive cancer phenotype has important consequences for IGF-1 signaling. Phosphorylated $Tyr^{1250/1251}$ could be a biomarker for identifying subsets of cancer that may not be targetable with antibodies targeting the receptor but may be amenable to other therapies that would target an IGF-1R signaling hub within the Golgi. Moreover, this phosphorylation site may distinguish IGF-1R and IR signaling in cells.

Materials and Methods

Cell culture, ligand stimulation, and pharmacological inhibitors

R- cells, MDA-MB-231 and HS578T cells were maintained in Dulbecco's Modified Eagles Medium (DMEM). Cal-51 were cultured in 50/50 mix of DMEM/Hams Nutrient F12 media. Prostate cancer DU-145 cells were cultured in RPMI 1640. Media were supplemented with 10% (v/v) heat inactivated fetal bovine serum, 10 mM L-Glutamine, with 5 mg/ml penicillin/streptomycin added. Cells were cultured at 37 °C in a humidified atmosphere at 5% CO2. All cells were determined to be free of mycoplasma by specific DNA staining and routinely maintained in culture for up to 6- 8 weeks for use in experiments.

For the analysis of IGF-1 stimulation in western blotting, cells were seeded 20 hr prior to starvation and allowed to reach approximately 70% confluency. Cells were serum-starved for 4 hr followed by stimulation with the indicated concentrations of IGF-1, IGF-2 or Insulin. Generally, R- cells transiently expressing the IGF-1R were stimulated with 10 ng/ml IGF-1 and cell lines with endogenous IGF-1R were stimulated with 50 ng/ml IGF-1.

For the analysis of detached cells (suspension), cells seeded on 10 cm plates were cultured overnight in complete medium and the starved from serum for 4 hr in total. After 3 hr cells were enzymatically detached and left in suspension for 1hr. Cells were then stimulated with IGF-1, centrifuged at 1000 rpm for 5 minutes, washed with PBS and lysed.

Kinase inhibitors BMS-754807 (Stratech/Selleckchem, cat# S1124-SEL;300 nM and 1000 nM) AP26113 (Stratech/Selleckchem; cat# S7000-SEL; 500 nM), PF-573228 (Tocris Bioscience,cat#3239-10; 9 μM) and PP2 (Sigma/Merk; cat#529573-5mg; 35 μM) were added to cells for the last hour of 4 hr serum starvation.

The proteosomal or lysosomal inhibitors MG-132 (Calbiochem, cat#474790; 10 μM, Leupeptin (Sigma/Merk; cat#L2884-25 mg; 2 μM), E64 (Sigma/Merk; cat#E3132-5mg; 2.6μM) and Chloroquine (CQ) (Cell Signalling, cat#14774; 50 μM) were added to cell cultures for 4 or 6

hr and the appropriate vehicle was added to controls (0 h). The Golgi disruptor Brefeldin A (Sigma/Merk; cat# B7651-5mg; 10 µg/ml) was added to cells in complete medium.

Generation and transfection of IGF-1R mutants

Cells were transiently transfected with pcDNA4 plasmid encoding the WT IGF-1R or Kinase dead (K1003R) mutant and pcDNA4 plasmid encoding IGF-1R WT, FF or EE mutants. R- cells, cells were seeded 24 hr prior to transfection at a density of approximately 1.0x 10^6 cells/10 cm plate. Lipofectamine 2000 (Invitrogen cat# 11668-019) diluted in OptiMem was used to transfect cells with relevant DNA plasmid (12-16 µg). After 24 hr cells were re-seeded for experiments at 48 hr post transfection.

MDA-MB-231, MCF-7 and DU-145 cells were seeded 24 hr prior to transfection to approximately 70% confluency in 6-well or 10 cm plates for transfection with Lipofectamine 2000. All cell lines were transfected with 2 µg/6 well plate and 12 µg/10 cm plate of pcDNA4 plasmid. Cells were re-seeded in new plates at 24 hr post transfection for subsequent experiments

IGF-1R mutants were generated using the Quick-Change Lightning SDM Kit (Agilent, #210518). The pcDNA4 plasmid encoding WT IGF-1R was used to generate the K1003R, Y1250/Y1251 to phenylalanine (FF) and glutamic acid (EE) mutants.

IGF-1R knock-out cells were generated using CRISPR technology. The IGF-1R Double Nickase Plasmid (h) (sc-400084-NIC) was obtained from Santa Cruz Biotechnologies, Inc. and transfection carried out as described by the supplier protocol. Selection of transfected cells was achieved using Puromycin (0.5 µg/ml for MDA-MB-231 and MCF-7 cells and 0.4 µg/ml for DU-145 cells). IGF-1R knock-out cell pools were selected by immunoblotting for IGF-1R and then cloned by serial dilution. IGF-1R knockout (KO) clones were also subsequently pooled to

ensure they represented the original cell cultures. These pools were used for stable transfection of pcDNA4 plasmids encoding the WT, FF or EE IGF-1R followed by selection in medium supplemented with 400 µg/ml Zeocin over 4 weeks.

SDS -PAGE and western blotting

Cells were washed with ice-cold PBS twice and lysed immediately with cold lysis buffer (20 mM Tris, pH 8, 50 mM NaCl, 50mM NaF, 1% NP40) containing protease and phosphatase inhibitors for 30 min on ice followed by centrifugation at 14.000 rpm for 15 min at 4˚C. Samples were denatured by boiling for 5 min with 5x SDS PAGE loading buffer Technical replicates of the same denatured samples (30 µg protein) were separated on 8-10% gels to enable analysis of distinct IGF-1R phospho-sites. Proteins were then transferred to nitrocellulose membranes that were blocked for 1hr at room temperature in 5% BSA in Tris-buffered saline-T (20 mM Tris, 150 mM NaCl and 0.05% Tween 20, pH 7.6 (TBS-T). Primary antibodies were diluted at 1/1000 or 1/10000 dilution for β-actin in TBS-T containing 5% milk or BSA and incubated with membranes at 4 °C overnight. To detect distinct IGF-1R phospho-sites each blot was incubated with rabbit phospho-IGF-1R or mouse/rabbit total IGF-1R antibodies and a mouse antibody detecting a protein input control (tubulin). For detection of p-Thr^{202}/Tyr^{204}/ERK, p-Ser^{473}/AKT and p-Tyr$^{239/240}$ blots were probed with a combination of rabbit antibody detecting the phosphorylated protein, a mouse antibody detecting the total protein, followed by mouse antibodies to detect the input control. IRDYE-conjugated secondary antibodies (1/10,000) were used for detection with the Odyssey Image Scanner System (LI-COR Biosciences). Image studio quantification software was used for densitometry. Each phospho-IGF-1R protein was

normalized to total IGF-1R, or first to the input control and then to total IGF-1R. Other phosphoproteins were normalized to their respective total protein.

Phospho-Tyr$^{1250/1251}$ antibody adsorption and IGF-1R phosphopetide array

The phospho-Tyr^{1250} IGF-1R (Santa Cruz cat#SC-293102, biorbyt cat#orb43345) was adsorbed to nitrocellulose membrane that were coated with non-phosphorylated SFYYS peptide. Membranes dotted with peptide were allowed to dry completely and blocked with PBS containing 1% BSA for 1 hr at RT. These membranes were then incubated with the phospho-Tyr^{1250} antibody for 1 hr rotating at RT and the antibody recovered for subsequent use in western blotting.

Custom-made Intavis CelluSpots Peptide arrays (cat #32.100) containing 18 amino acid peptide sequences of the IGF-1R and the IR encompassing specific tyrosines and serines phosphorylated or non-phosphorylated immobilized on glass arrays were used to analyze the specificity of the commercial p-Tyr^{1250} IGF-1R antibody. The phospho-Tyr^{1250} antibody (1/500) was incubated with slides that were subsequently processed in the same way as western blots.

Immunoprecipitation and in vitro kinase assays

Cells were lysed and 0.5-1 mg of protein lysate was incubated with antibodies detecting IGF-IR (IGF-IRβ Antibody (C-20) cat# sc-713 Santa Cruz, IGF-1Rα Antibody (αIR3) cat#GR11L, Merk, IGF-IRβ Antibody cat#3027 Cell Signalling) at 1/100 dilution overnight rotating at 4˚C. Immune complexes were obtained by adding 50 µl of pre-washed Protein G-Agarose beads to the antibody-lysate mix for 2 hr at 4˚C. Beads were washed three times using lysis buffer and loading dye was added to the washed beads (2x) before samples were boiled for 5 mins at 95˚C,

centrifuged at 14.000 rpm for 2 min followed by SDS PAGE and western blotting. To investigate multiple IGF-1R phospho-sites, denatured samples were split for two sets of gels. The antibody detecting the phospho-site was then removed using stripping buffer (200 mM NaOH with 1% SDS) and incubated with total IGF-1R (1/1000).

The ADP-Glo^{TM} Kinase Assay kit (Promega) was used for in-vitro kinase assays. For kinase assay protein input to immunoprecipitations of IGF-1R WT and FF were adjusted to be equivalent to EE. Beads with immunoprecipitated IGF-1R were washed twice with kinase buffer (40 mM Tris (pH 7.5), 20 mM MgCl2, 2 mM MnCl2, 0.1 mg/ml BSA, 2 mM DTT, 100 uM Sodium Vanadate) and then incubated with kinase buffer containing 150 µM ATP (ADP-GloTM Kinase Assay) and 2 mg/ml poly(Glu, Tyr) (4:1) (P0275; Sigma) as an exogenous substrate for 30 min, with samples mixed every 10 min. Beads were centrifuged for 30 sec at 14,000 rpm and triplicates (5 µl) of supernatant were added to a white 384-well plate for incubation with ADP-Glo (5 µl per sample) for 60 min at room temperature. The ADP-Glo Kinase detection reagent (10 µl) was added to each reaction for 30 min at room temperature, and kinase activity measured with a luminometer (BioTek)

Mass spectrometry

Mass Spectrometry for phospho-peptide mapping of the IGF-1R was carried out at the FingerPrints Proteomics Facility the University of Dundee. IGF-1R was immunoprecipitated from R- cells transfected with pcDNA3 IGF-1R WT and that were either serum-starved or stimulated with IGF-1 were transferred as protein G agarose-bound protein precipitates to the Dundee facility where they were subjected to Trypsin/AspN digestion and enrichment of

phosphor-peptides by titanium dioxide. Mass Spectrometry was performed using an Orbitrap Velos system.

Quantitative PCR

R- cells transiently expressing WT, FF or EE IGF-1R were prepared for RNA extraction 48 hr post-transfection. RNA was extracted using the PureLink RNA Mini Kit (Thermo Scientific) according to the manufacturer's protocol. To synthesize cDNA, 1 µg of RNA and the QuantiTect reverse transcription kit (Qiagen) was used. Quantitative PCR was performed using the Roche FastStart essential DNA Green Master Kit and the Lightcycler 96 Instrument (Roche Diagnostics). Actin was used as housekeeping control. The 2 CT method was used to analyze data and to determine relative mRNA expression levels. IGF-1R mRNA expression values were normalized to actin and expressed as fold-change relative to the WT IGF-1R (set to 1). The following primer set was used to detect IGF-1R: Forward-5' ATGTCCAGGCCAAACAGGAT'3 and Reverse: 5'CCTCCCACTCATCAGGAACG'3.

Immunofluorescence

Cells were cultured on 12mm glass coverslips, washed with phosphate-buffered saline, fixed with 4% paraformaldehyde in PHEM buffer for 60 min at room temperature, quenched with 50 mM Ammonium Chloride for 20 min, and permeabilized using 0.1% Triton/PHEM for 5 min. PHEM buffer containing donkey serum (10%) was used for blocking and dilution of antibodies. Coverslips were incubated with primary antibodies at 4˚C, washed with PHEM 3 times followed by secondary antibodies and Hoechst dye to stain nuclei. The following reagents were used: IGF-1 Receptor in mouse cells Cell Signalling antibody cat# 9750 (1/200), for human cells cat#

3027 (1/200 for MCF-7 cells, 1/100 for other cell lines); the cis Golgi apparatus: GM130 (D cat#610822 (1/200): *cis*- and *trans*-Golgi network: biotinylated Vicia Villosa (VVA; Lectin Vector Laboratories cat#B-1235-2) (1/400). Cy3-conjugated AffiniPure Donkey Anti-Mouse antibody (1/1000), Alexa Fluor 488-conjucated AffiniPure Donkey (1/200), Alexa Fluor 594-conjucated Streptavidin (1/1000) and Alexa Fluor 488-conjucated Streptavidin (1/200) were used for detection of primary antibodies. Phalloidin (TRITC Sigma cat# P1951 or AlexaFluor 405 ThermoFisher cat# A30104) was used to detect Actin, and Hoechst was used to stain nuclei.

To assess internalization of activated IGF-1R, cells were serum-starved for 4 hr and incubated with the IGF-1R α-chain (IRα) antibody for 30 min either on ice or at 37°C. Cells were then fixed and stained with an antibody detecting the IGF-1R β-chain (green). Cells were then incubated with secondary antibodies detecting either the IRα (red) or IGF-1R (green). IRα antibody bound or internalized with surface-located IGF-1R appeared yellow.

Images were acquired using a SPOT charge-coupled device camera mounted on a Nikon T600 fluorescent microscope or a Nikon DSFi1c camera attached to the Leica DM LB2 microscope. For confocal microscopy, images were acquired using an Olympus Flouview FV1000 confocal laser scanning microscope (numerical aperture: 1.4) with a 60x-immersion objective. Maximum intensity projections and z-stacks were processed in Image J. Brightness and contrast were adjusted in Adobe Photoshop if needed. To determine fluorescence intensity within the cells, ImageJ software was used to determine fluorescence signal intensity within the cells.

In-cell western assays for IGF-1R

Cells were seeded at $5x10^4$ cells per well in 96-well tissue culture plates in complete medium for 24 hr, washed three times with PBS, serum-starved for 4 hr followed by stimulation with 10

ng/ml IGF-1 for 10 min or left in serum-free medium or complete medium. Cells were immediately fixed with 100 µl of a freshly prepared fixing solution (4% formaldehyde/PHEM) and incubated at room temperature for 30 min followed by quenching with 50 mM Ammonium Chloride for 20 min and washing with PHEM. Cells in wells with complete medium, or incubated with p-AKT/AKT and one 3x set of the secondary control antibody were permeabilized using 0.1% Triton/PHEM for 5 min and washed with PHEM. All wells were then blocked for 1 hr with 50 µl of blocking buffer (5% goat serum/PHEM). Primary antibody (IGF-1R IR3 for surface and Cell Signaling IGF-1Rβ cat#3027, or p- Ser^{473}/AKT) was added for 2 hr with gentle rocking followed by washing and incubation with secondary antibody. Goat anti-Mouse IRdye® 680 (1/1000) (Odyssey infrared imaging system; cat#926-32220) or Goat anti-Rabbit IRDye® 800 (1/1000) (Odyssey infrared imaging system; cat#926-32211) were used to detect primary antibodies. Syto60 (Invitrogen) was also included (1:10,000) as a cell-permeable nucleic acid stain that fluoresces at 680 nm and was detected using the Odyssey infrared scanner. Cells were washed five times with PHEM. Plates were dried, and IGF-1R (surface and total levels) intensity was quantified using the Image studio quantification software with normalization to Syto60 levels.

Cell migration assays

HS578T cells were seeded in Culture-Insert 2 well 35 mm plates (ibidi Gmbh cat# 81176) ($4.0x10^5$ cells/ml,70 µl per well). Cells were allowed to attach for 24 hr in serum-free medium containing either DMSO (vehicle) or the Golgi disruptor BFA (10 µg/ml) for four hours. The wound was generated by removal of the insert and the medium in respective dishes was then supplemented with IGF-1 (50 ng/ml). Wounds were photographed with a Nikon charge-coupled

device camera connected with the Nikon Eclipse TE 300 microscope (10x magnification) after 0 hr and 6 hr of migration. For immunofluorescence HS578T cells were seeded in Culture-Insert 2 well inserts on coverslips (ibidi Gmbh cat# 80209) and allowed to attach for 24 hr. The wound area was photographed with a Nikon charge-coupled device camera connected with the Nikon Eclipse TE 300 microscope at 0 hr and 6 hr of migration. Subsequently, coverslips were recovered for immunofluorescence.

Statistical analysis

Western blot densitometry results were expressed as fold-change in the ratio of phospho/total protein relative to the control condition (set to 1), which is indicated as a white bar in each graph. For calculations comparing fold-change of each group to the control, one-sample *T*-tests were used to test the null hypothesis that the expected ratio was 1. For calculations comparing fold change of groups (≠ control condition) independent two-sample *T*-tests were used. *P*-values were adjusted using Benjamini-Hochberg correction for multiple testing. A 3x3 ANOVA was conducted to examine the main effects of Group and Condition, and the interaction between Group and Condition in Fig 4A. Statistical significance was determined using P-value<0.05 and all tests were two-tailed.

Supplementary Materials

Fig. S1 Immunoreactivity of phosphorylated Tyr^{1250} IGF-1R antibody

Fig. S2. Protein abundance and mRNA expression for wild-type and mutant IGF-1Rs stably expressed in R- cells

Fig. S3. WT and EE IGF-1R internalize in large vesicles upon IRα antibody binding

References and Notes

1. J. P. Liu, J. Baker, A. S. Perkins, E. J. Robertson, A. Efstratiadis, Mice carrying null mutations of the genes encoding insulin-like growth factor I (Igf-1) and type 1 IGF receptor (Igf1r). *Cell* **75**, 59-72 (1993).
2. M. Pollak, The insulin and insulin-like growth factor receptor family in neoplasia: an update. *Nature Reviews Cancer* **12**, 159 (2012).
3. E. Osher, V. M. Macaulay, Therapeutic Targeting of the IGF Axis. *Cells* **8**, 895 (2019).
4. V. P. Brahmkhatri, C. Prasanna, H. S. Atreya, Insulin-like growth factor system in cancer: novel targeted therapies. *Biomed Res Int* **2015**, 538019-538019 (2015).
5. P. F. Christopoulos, P. Msaouel, M. Koutsilieris, The role of the insulin-like growth factor-1 system in breast cancer. *Molecular cancer* **14**, 43-43 (2015).
6. A. Arcaro, Targeting the insulin-like growth factor-1 receptor in human cancer. *Front Pharmacol* **4**, 30-30 (2013).
7. M. Niepel *et al.*, Profiles of Basal and stimulated receptor signaling networks predict drug response in breast cancer lines. *Science signaling* **6**, ra84 (2013).
8. O. T. Cox *et al.*, IGF-1 Receptor and Adhesion Signaling: An Important Axis in Determining Cancer Cell Phenotype and Therapy Resistance. *Frontiers in Endocrinology* **6**, (2015).
9. A. M. Nagle *et al.*, Loss of E-cadherin Enhances IGF1–IGF1R Pathway Activation and Sensitizes Breast Cancers to Anti-IGF1R/InsR Inhibitors. *Clinical Cancer Research* **024**, 5165-5177 (2018).
10. I. Bajrami *et al.*, E-Cadherin/ROS1 Inhibitor Synthetic Lethality in Breast Cancer. *Cancer Discovery* **8**, 498-515 (2018).
11. A. Belfiore *et al.*, A novel functional crosstalk between DDR1 and the IGF axis and its relevance for breast cancer. *Cell Adhesion & Migration* **12**, 305-314 (2018).
12. U. Hermanto, C. S. Zong, W. Li, L.-H. Wang, RACK1, an Insulin-Like Growth Factor I (IGF-I) Receptor-Interacting Protein, Modulates IGF-I-Dependent Integrin Signaling and Promotes Cell Spreading and Contact with Extracellular Matrix. *Molecular and Cellular Biology* **22**, 2345-2365 (2002).
13. P. A. Kiely, G. S. Baillie, M. J. Lynch, M. D. Houslay, R. O'Connor, Tyrosine 302 in RACK1 Is Essential for Insulin-like Growth Factor-I-mediated Competitive Binding of PP2A and β1 Integrin and for Tumor Cell Proliferation and Migration. *Journal of Biological Chemistry* **283**, 22952-22961 (2008).
14. P. A. Kiely, M. Leahy, D. O'Gorman, R. O'Connor, RACK1-mediated Integration of Adhesion and Insulin-like Growth Factor I (IGF-I) Signaling and Cell Migration Are Defective in Cells Expressing an IGF-I Receptor Mutated at Tyrosines 1250 and 1251. *Journal of Biological Chemistry* **280**, 7624-7633 (2005).
15. V. A. Blakesley, A. P. Koval, B. S. Stannard, A. Scrimgeour, D. LeRoith, Replacement of Tyrosine 1251 in the Carboxyl Terminus of the Insulin-like Growth Factor-I Receptor Disrupts the Actin Cytoskeleton and Inhibits Proliferation and Anchorage-independent Growth. *Journal of Biological Chemistry* **273**, 18411-18422 (1998).
16. M. Miura, E. Surmacz, J.-L. Burgaud, R. Baserga, Different Effects on Mitogenesis and Transformation of a Mutation at Tyrosine 1251 of the Insulin-like Growth Factor I Receptor. *Journal of Biological Chemistry* **270**, 22639-22644 (1995).
17. R. O'Connor *et al.*, Identification of domains of the insulin-like growth factor I receptor that are required for protection from apoptosis. *Molecular and cellular biology* **17**, 427-435 (1997).
18. P. Brodt, L. Fallavollita, A.-M. Khatib, A. A. Samani, D. Zhang, Cooperative Regulation of the Invasive and Metastatic Phenotypes by Different Domains of the Type I Insulin-like Growth Factor Receptor β Subunit. *Journal of Biological Chemistry* **276**, 33608-33615 (2001).
19. M. Leahy, A. Lyons, D. Krause, R. O'Connor, Impaired Shc, Ras, and MAPK Activation but Normal Akt Activation in FL5.12 Cells Expressing an Insulin-like Growth Factor I Receptor Mutated at Tyrosines 1250 and 1251. *Journal of Biological Chemistry* **279**, 18306-18313 (2004).
20. G. M. Kelly, D. A. Buckley, P. A. Kiely, D. R. Adams, R. O'Connor, Serine Phosphorylation of the Insulin-like Growth Factor I (IGF-1) Receptor C-terminal Tail Restrains Kinase Activity and Cell Growth. *Journal of Biological Chemistry* **287**, 28180-28194 (2012).
21. V. A. Blakesley *et al.*, Tumorigenic and mitogenic capacities are reduced in transfected fibroblasts expressing mutant insulin-like growth factor (IGF)-I receptors. The role of tyrosine residues 1250, 1251, and 1316 in the carboxy-terminus of the IGF-I receptor. *Endocrinology* **137**, 410-417 (1996).

22. H. Zheng *et al.*, Selective recruitment of G protein-coupled receptor kinases (GRKs) controls signaling of the insulin-like growth factor 1 receptor. *Proceedings of the National Academy of Sciences* **109**, 7055-7060 (2012).
23. J. Stanicka *et al.*, FES-related tyrosine kinase activates the insulin-like growth factor-1 receptor at sites of cell adhesion. *Oncogene* **37**, 3131-3150 (2018).
24. L. Taliaferro-Smith *et al.*, FAK activation is required for IGF1R-mediated regulation of EMT, migration, and invasion in mesenchymal triple negative breast cancer cells. *Oncotarget* **6**, 4757-4772 (2015).
25. W. D. Mahauad-Fernandez, C. M. Okeoma, Cysteine-linked dimerization of BST-2 confers anoikis resistance to breast cancer cells by negating proapoptotic activities to promote tumor cell survival and growth. *Cell Death & Disease* **8**, e2687-e2687 (2017).
26. L. Johannes, V. Popoff, Tracing the Retrograde Route in Protein Trafficking. *Cell* **135**, 1175-1187 (2008).
27. Q.-H. Ye *et al.*, GOLM1 Modulates EGFR/RTK Cell-Surface Recycling to Drive Hepatocellular Carcinoma Metastasis. *Cancer Cell* **30**, 444-458 (2016).
28. J. Lippincott-Schwartz, L. C. Yuan, J. S. Bonifacino, R. D. Klausner, Rapid redistribution of Golgi proteins into the ER in cells treated with brefeldin A: Evidence for membrane cycling from Golgi to ER. *Cell* **56**, 801-813 (1989).
29. A. A. Samani, S. Yakar, D. LeRoith, P. Brodt, The Role of the IGF System in Cancer Growth and Metastasis: Overview and Recent Insights. *Endocrine Reviews* **28**, 20-47 (2007).
30. V. Millarte, H. Farhan, The Golgi in Cell Migration: Regulation by Signal Transduction and Its Implications for Cancer Cell Metastasis. *The Scientific World Journal* **2012**, 11 (2012).
31. D. A. Ucar *et al.*, Disruption of the protein interaction between FAK and IGF-1R inhibits melanoma tumor growth. *Cell Cycle* **11**, 3250-3259 (2012).
32. J. E. Peterson *et al.*, Src Phosphorylates the Insulin-like Growth Factor Type I Receptor on the Autophosphorylation Sites: REQUIREMENT FOR TRANSFORMATION BY src. *Journal of Biological Chemistry* **271**, 31562-31571 (1996).
33. B. B. M. Flossmann-Kast, P. M. Jehle, A. Hoeflich, G. Adler, M. P. Lutz, Src Stimulates Insulin-like Growth Factor I (IGF-I)-dependent Cell Proliferation by Increasing IGF-I Receptor Number in Human Pancreatic Carcinoma Cells. *Cancer Research* **58**, 3551-3554 (1998).
34. Y. Yoneyama *et al.*, IRS-1 acts as an endocytic regulator of IGF-I receptor to facilitate sustained IGF signaling. *eLife* **7**, e32893 (2018).
35. C. M. Warren, S. Ziyad, A. Briot, A. Der, M. L. Iruela-Arispe, A Ligand-Independent VEGFR2 Signaling Pathway Limits Angiogenic Responses in Diabetes. *Science signaling* **7**, ra1-ra1 (2014).
36. A. Disanza, E. Frittoli, A. Palamidessi, G. Scita, Endocytosis and spatial restriction of cell signaling. *Molecular Oncology* **3**, 280-296 (2009).
37. N. M. Frazier, T. Brand, J. D. Gordan, J. Grandis, N. Jura, Overexpression-mediated activation of MET in the Golgi promotes HER3/ERBB3 phosphorylation. *Oncogene* **38**, 1936-1950 (2019).
38. Y. Obata *et al.*, Oncogenic Kit signalling on the Golgi is suppressed by blocking secretory trafficking with M-COPA in gastrointestinal stromal tumours. *Cancer Letters* **415**, 1-10 (2018).
39. Y. Obata *et al.*, Oncogenic signaling by Kit tyrosine kinase occurs selectively on the Golgi apparatus in gastrointestinal stromal tumors. *Oncogene* **36**, 3661-3672 (2017).
40. Z. Xiang, F. Kreisel, J. Cain, A. Colson, M. H. Tomasson, Neoplasia Driven by Mutant c-KIT Is Mediated by Intracellular, Not Plasma Membrane, Receptor Signaling. *Molecular and Cellular Biology* **27**, 267-282 (2007).
41. S. Tabone-Eglinger *et al.*, KIT Mutations Induce Intracellular Retention and Activation of an Immature Form of the KIT Protein in Gastrointestinal Stromal Tumors. *Clinical Cancer Research* **14**, 2285-2294 (2008).
42. H. Bougherara *et al.*, The Aberrant Localization of Oncogenic Kit Tyrosine Kinase Receptor Mutants Is Reversed on Specific Inhibitory Treatment. *Molecular Cancer Research* **7**, 1525-1533 (2009).
43. L. Citores, L. Bai, V. Sørensen, S. Olsnes, Fibroblast growth factor receptor-induced phosphorylation of STAT1 at the golgi apparatus without translocation to the nucleus. *Journal of Cellular Physiology* **212**, 148-156 (2007).
44. T. Aleksic *et al.*, Nuclear IGF1R Interacts with Regulatory Regions of Chromatin to Promote RNA Polymerase II Recruitment and Gene Expression Associated with Advanced Tumor Stage. *Cancer Research* **78**, 3497-3509 (2018).
45. T. Aleksic *et al.*, Type 1 insulin-like growth factor receptor translocates to the nucleus of human tumor cells. *Cancer research* **70**, 6412-6419 (2010).

46. H. Deng *et al.*, Over-accumulation of nuclear IGF-1 receptor in tumor cells requires elevated expression of the receptor and the SUMO-conjugating enzyme Ubc9. *Biochemical and Biophysical Research Communications* **404**, 667-671 (2011).
47. J. H. Law *et al.*, Phosphorylated Insulin-Like Growth Factor-I/Insulin Receptor Is Present in All Breast Cancer Subtypes and Is Related to Poor Survival. *Cancer Research* **68**, 10238-10246 (2008).
48. Y. Perez-Riverol *et al.*, The PRIDE database and related tools and resources in 2019: improving support for quantification data. *Nucleic Acids Research* **47**, D442-D450 (2018).

Acknowledgments: We would like to acknowledge Dr. Janina Berghoff, Dr. Michael Coleman, Dr. Deirdre Buckley, Ms. Aoife O'Connell and Mr. Moritz Hirsch for assistance with site directed mutagenesis, peptides, and transfections. We also acknowledge Dr. Orla Cox and Dr. Nancy Kedersha for assistance with immunofluorescence. We thank Dr. Kathleen O'Sullivan from the School of Mathematical Sciences for advice on statistical analyses and colleagues in the Department of Biochemistry and Cell Biology for helpful suggestions. We also thank Mr. Douglas Lamont of the FingerPrints Proteomics Facility at the University of Dundee, which is supported by the 'Wellcome Trust Technology Platform' award [097945/B/11/Z]. In addition, we thank colleagues in the Department of Biochemistry and Cell Biology for helpful suggestions. **Funding**: This work was funded by Science Foundation Ireland Principal Investigator Awards 16/A/4505 and 11/PI/1139. **Author contributions**: LR, SO'S, GG and GK contributed to conception and design of experiments, acquisition and interpretation of data, and drafting the manuscript. RO'C contributed to conception design, interpretation of data and drafting the article. **Competing interests**: The authors declare that they have no competing interests. **Data and Materials Availability**: The mass spectrometry proteomics data have been deposited to the ProteomeXchange Consortium via the PRIDE partner repository (*48*) with the dataset identifier PXD017644. All other data needed to evaluate the conclusions in the paper are present in the paper or the Supplementary Materials.

A

Sample	Site	Sequence	Ion Score >19
Serum Starved	1248/1250/1251/1252	EVSFYYSEENK	27
IGF-1 10 min	943/945/950/952/957	LGNGVLYASVN PEYFSAADVYVP DEWEVAREK	39
	1131	DIYETDYYRK	28
	1131/1135/1136	DIYETDYYRK	26
	1248/1250/1251/1252	EVSFYYSEENK	49

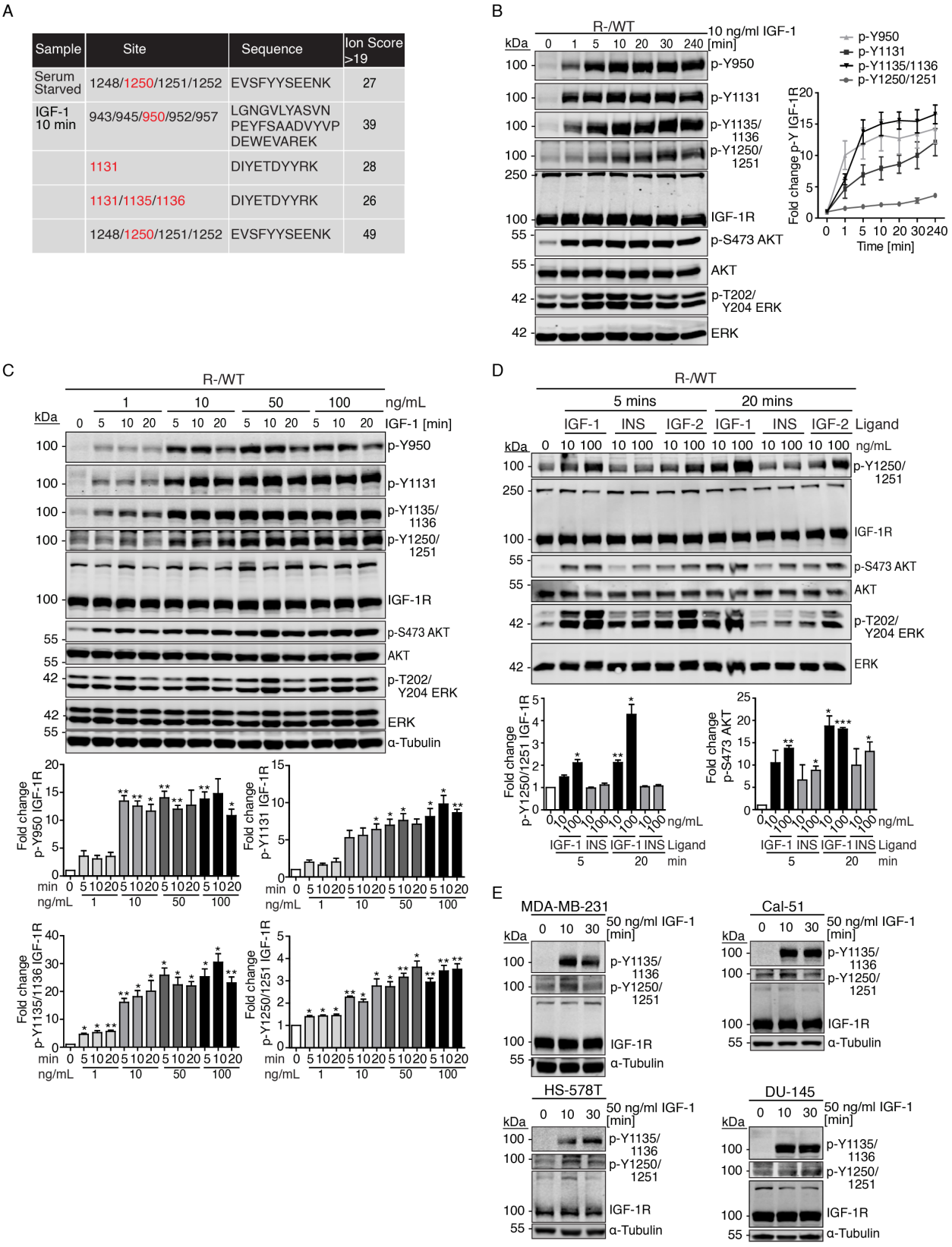

Fig. 1. **Tyr$^{1250/1251}$ phosphorylation in cells.** (**A**) Phophopeptides identified by mass spectroscopy from IGF-1R immunoprecipitated from R- cells stably expressing WT IGF-1R (R-/WT cells) following serum starvation or exposure to IGF-1. Phosphorylated (p-) IGF-1R tyrosines are indicated in red. (**B**) Immunoblotting for and quantification of the indicated phosphotyrosines (p-Y) in IGF-1R, the indicated phosphorylated forms of AKT and ERK, and total IGF-1R, AKT, and ERK from whole lysates of R-/WT cells. Total AKT and ERK, are loading controls. Phosphotyrosine-containing proteins were quantified by densitometry, normalized to the protein loading control (total AKT, total ERK and IGF-1R) and presented as average fold-change ± SEM in the ratio of phosphorylated/total protein relative to the control condition (set to 1). (**C**) Immunoblotting for and quantification of the indicated phosphorylated forms of IGF-1R, total IGF-1R, ERK phosphorylated on Tyr^{202} and Tyr^{204} (p-T202/Y204), and total ERK from R-/WT cells stimulated with IGF-1 at the indicated concentrations and times following serum starvation. Quantification of phosphorylated/total IGF-1R is expressed as average fold-change ± SEM relative to the control condition (set to 1). Significance was calculated using a two-sided one-sample *T*-test. (**D**) Immunoblotting for and quantification of phosphorylated Tyr$^{1250/1251}$ in IGF-1R (p-Y1250/1251), total IGF-1R, AKT phosphorylated at Ser^{473}, total AKT, ERK phosphorylated at Thr^{202} and Tyr^{204}, and total ERK from R-/WT cells stimulated with IGF-1, IGF-2, or insulin (INS). Densitometry quantification is presented as the average fold-change ± SEM in the ratio of phosphorylated/total protein relative to the control condition. Significance was calculated using a two-sided one-sample *T*-test. (**E**) Immunoblotting for IGF-1R phosphorylated on Tyr$^{1135/1136}$ (p-Y1135/1136), Tyr$^{1250/1251}$, and total IGF-1R from cancer cells serum-starved and stimulated with IGF-1. For all experiments, blots are

representative of n≥ 3 independent experiments, and densitometry data was derived from 3 or more independent experiments. *P*-values, *<0.05, **<0.01, ***<0.001.

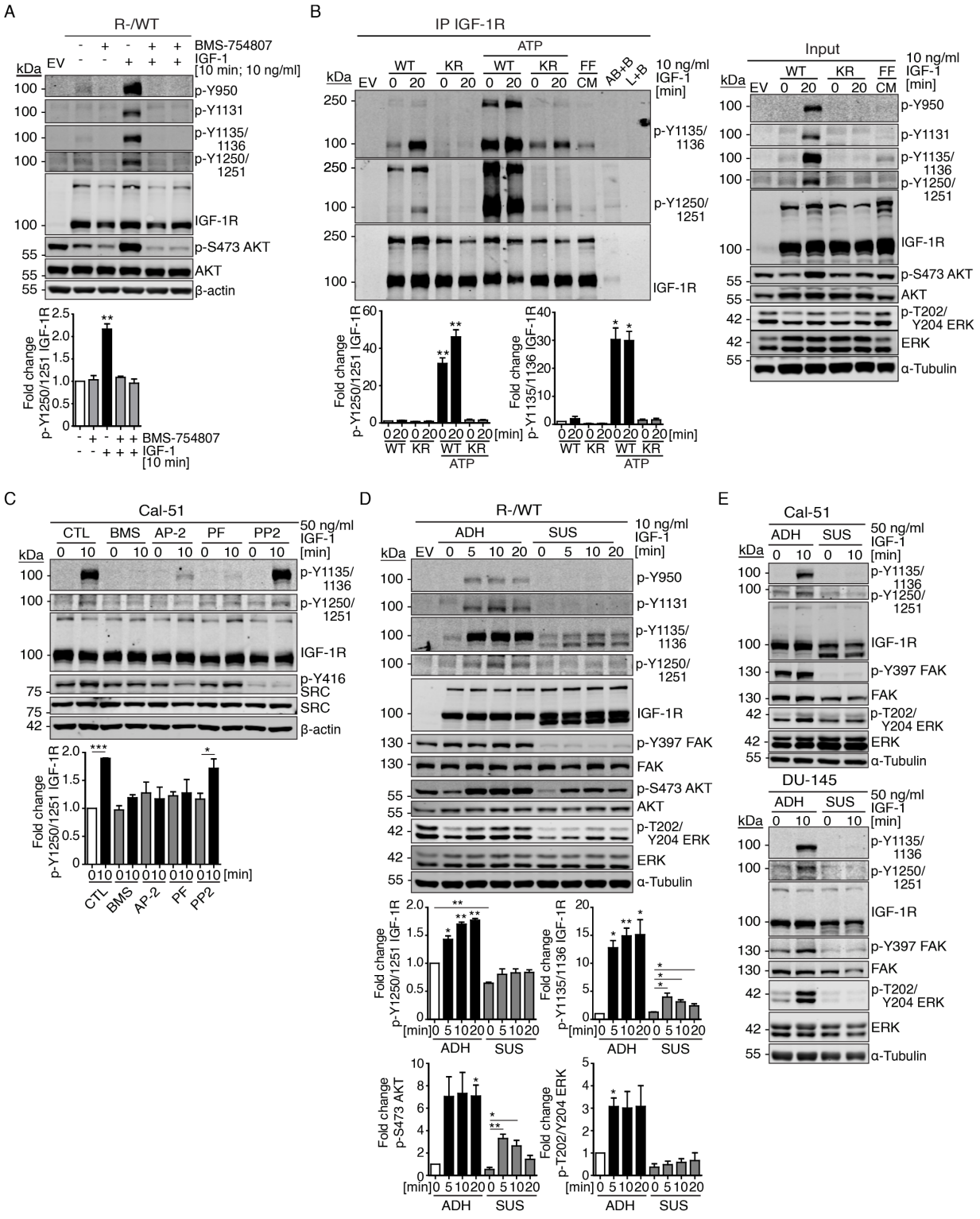

Fig. 2. Adhesion signals and IGF-1R kinase activity promote Tyr$^{1250/1251}$ phosphorylation.

(A) Immunoblot of the indicated phosphorylated forms of IGF-1R and total IGF-1R from whole

cell lysates of R- cells transiently expressing empty vector (EV) or WT IGF-1R (R-/WT cells) that were serum-starved followed by stimulation with IGF-1 for the indicated times. Cells were incubated with BMS-754807 for 1 hr prior to IGF-1 stimulation as indicated. Phosphorylated $Tyr^{1250/1251}$ IGF- 1R was quantified by densitometry. (**B**) Immunoblotting for the total IGF-1R and indicated phosphorylated forms of IGF-1R immunoprecipitated from R- cells expressing either empty vector, WT IGF-1R or KR mutant IGF-1R that were serum-starved and stimulated with IGF-1, or FF mutant cultured in complete medium (CM). AB+B (antibody plus beads) and L+B (cell lysate plus beads) are negative controls for immunoprecipitation. Immunoprecipitates were incubated with kinase buffer containing ATP or not. IGF- 1R phosphorylated on $Tyr^{1250/1251}$ and on $Tyr^{1135/1136}$ were quantified by densitometry. Protein input is shown in immunoblots for phosphorylated and total IGF-1R, AKT, and ERK. (**C**) Immunoblotting for and analysis of the indicated phosphorylated forms of IGF-1R and Src, total IGF-1R, and total Src from Cal-51 cells that were serum-starved, exposed to kinase inhibitors [BMS, BMS-754807 (IGF-1R inhibitor); AP-2, AP-26113 (FER inhibitor); PF, PF573228 (FAK inhibitor); PP2 (Src inhibitor)], then stimulated with IGF-1. IGF-1R phosphorylated on $Tyr^{1250/1251}$ IGF- 1R was quantified by densitometry. (**D**) Immunoblotting for the indicated phosphorylated forms of IGF-1R, FAK, AKT, and ERK and total IGF-1R, FAK, AKT, and ERK from adherent (ADH) and suspension-cultured (SUS) R- /WT cells stimulated with IGF-1 for the indicated times following serum starvation. The amounts of IGF- 1R phosphorylated on $Tyr^{1250/1251}$ and on $Tyr^{1135/1136}$, AKT phosphorylated on Ser^{473}, and ERK phosphorylated on Thr^{202}/Tyr^{204} were quantified by densitometry. (**E**) Immunoblotting for the indicated phosphorylated forms of IGF- 1R, FAK, and ERK and total IGF-1R, FAK, and ERK in adherent and suspension-cultured Cal-51 cells serum-starved and stimulated with IGF-1. For all experiments, densitometric quantification is presented

as average fold-change ± SEM in the ratio of phosphorylated/total protein relative to the control condition. Significance was calculated using a two-sided one-sample or two-sample *T*-test. n≥3 independent experiments. *P*-values, *<0.05, **<0.01, ***<0.001.

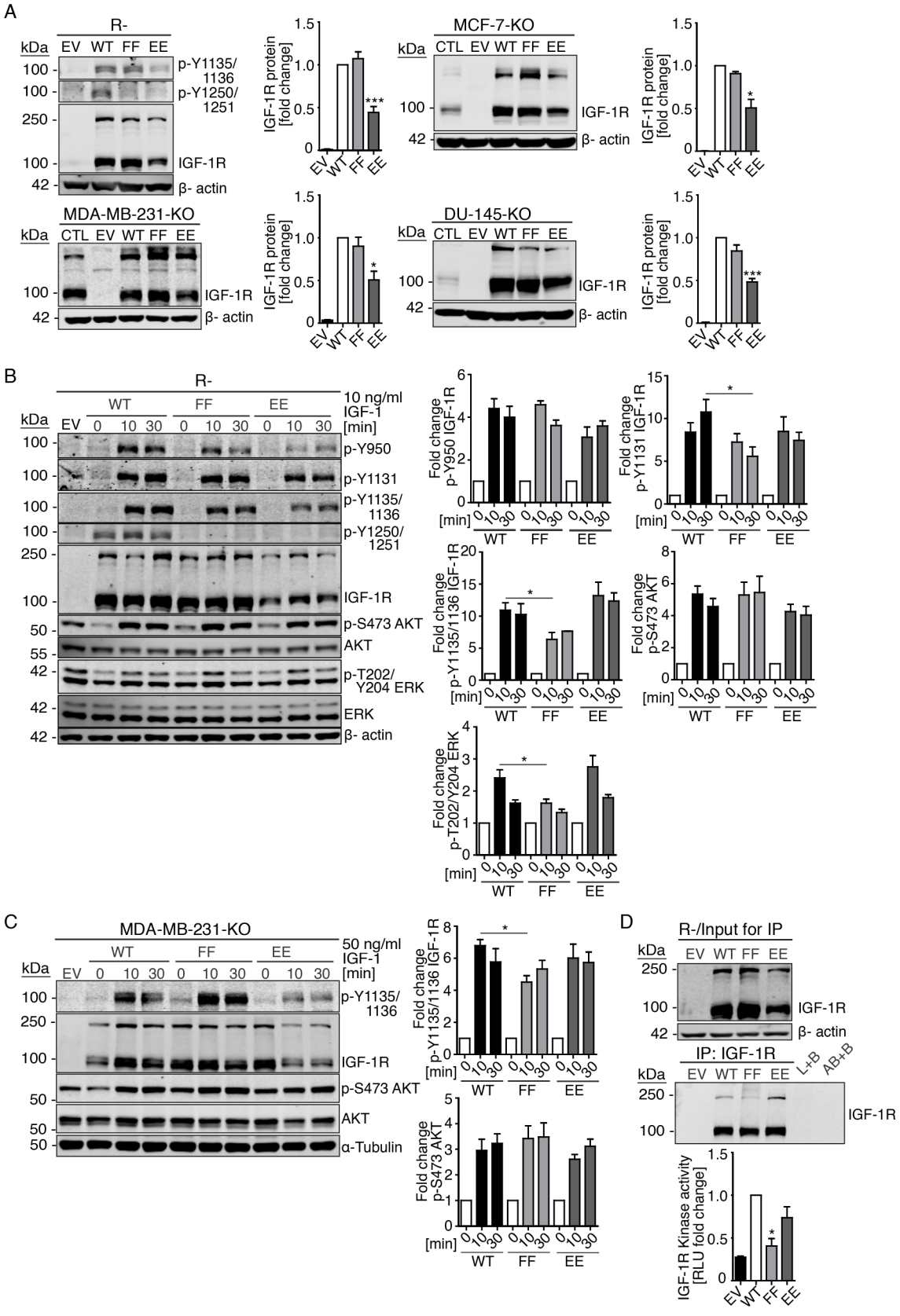
A
R-
kDa
EV WT FF EE
100
p-Y1135/ 1136
100
p-Y1250/ 1251
250
100
IGF-1R
42
β- actin
IGF-1R protein [fold change]
1.5
1.0
0.5
0
***
EV WT FF EE
MCF-7-KO
kDa
CTL EV WT FF EE
100
IGF-1R
42
β- actin
*
MDA-MB-231-KO
kDa
CTL EV WT FF EE
100
IGF-1R
42
β- actin
DU-145-KO
kDa
CTL EV WT FF EE
100
IGF-1R
42
β- actin
***
B
R-
10 ng/ml IGF-1
WT FF EE
kDa
EV 0 10 30 0 10 30 0 10 30
[min]
100
p-Y950
100
p-Y1131
100
p-Y1135/ 1136
100
p-Y1250/ 1251
250
100
IGF-1R
50
p-S473 AKT
55
AKT
42
p-T202/ Y204 ERK
42
ERK
42
β- actin
Fold change p-Y950 IGF-1R
Fold change p-Y1131 IGF-1R
Fold change p-Y1135/1136 IGF-1R
Fold change p-S473 AKT
Fold change p-T202/Y204 ERK
[min] 0 10 30
WT FF EE
C
MDA-MB-231-KO
50 ng/ml IGF-1
WT FF EE
kDa
EV 0 10 30 0 10 30 0 10 30
[min]
100
p-Y1135/ 1136
250
100
IGF-1R
50
p-S473 AKT
50
AKT
50
α-Tubulin
Fold change p-Y1135/1136 IGF-1R
Fold change p-S473 AKT
[min] 0 10 30
WT FF EE
D
R-/Input for IP
kDa
EV WT FF EE
250
100
IGF-1R
42
β- actin
IP: IGF-1R
kDa
EV WT FF EE L+B AB+B
250
100
IGF-1R
IGF-1R Kinase activity [RLU fold change]
1.5
1.0
0.5
0
*
EV WT FF EE

Fig. 3. Exogenously expressed Tyr$^{1250/1251}$ phosphomimetic (EE) IGF-1R is fully active. (**A**) Immunoblot of the indicated phosphorylated forms of IGF- 1R and total IGF-R1 in R- cells and total IGF-1R in IGF-1R knockout (KO) MCF-7, MDA-MB-231, and DU-145 cells transiently expressing the WT, FF (Tyr$^{1250/1251}$ not phosphorylatable), or EE (Tyr$^{1250/1251}$ phosphomimetic) forms of IGF-1R. (**B**) Immunoblotting for the indicated phosphorylated forms of IGF-1R, AKT, and ERK and total IGF-1R, AKT, and ERK from R- cells transiently overexpressing the WT, FF, or EE form of IGF-1R and stimulated with IGF-1 for the indicated times following serum starvation. Significance was calculated using a two-sided two-sample *T*-test. (**C**) Immunoblot of the indicated phosphorylated forms of IGF-1R and AKT and total IGF-1R and AKT in IGF-1R KO MDA-MB-231 cells transiently overexpressing IGF-1R WT, FF, or EE and stimulated with IGF-1 for the indicated times following serum starvation. For (A), (B), and (C) densitometry quantification is presented as the average fold-change ± SEM in ratio of phosphorylated/total protein relative to the control condition. n≥3 independent experiments. Significance was calculated using a two-sided two-sample *T*-test. (**D**) Immunoblot of total IGF-1R from R- cells transiently overexpressing IGF-1R WT, FF, or EE used to determine protein input to immunoprecipitate for in vitro kinase assays followed by immunoblotting of immunoprecipitated IGF-1R (all adjusted to EE protein amounts). Kinase assay data are presented as average fold-change ± SEM in kinase activity (measured in relative luciferase units: RLU) relative to control condition (IGF-1R WT). n=3 independent kinase preparations. Significance was calculated using two-sided one-sample *T*-test. *P*-values, *<0.05, **<0.01, ***<0.001.

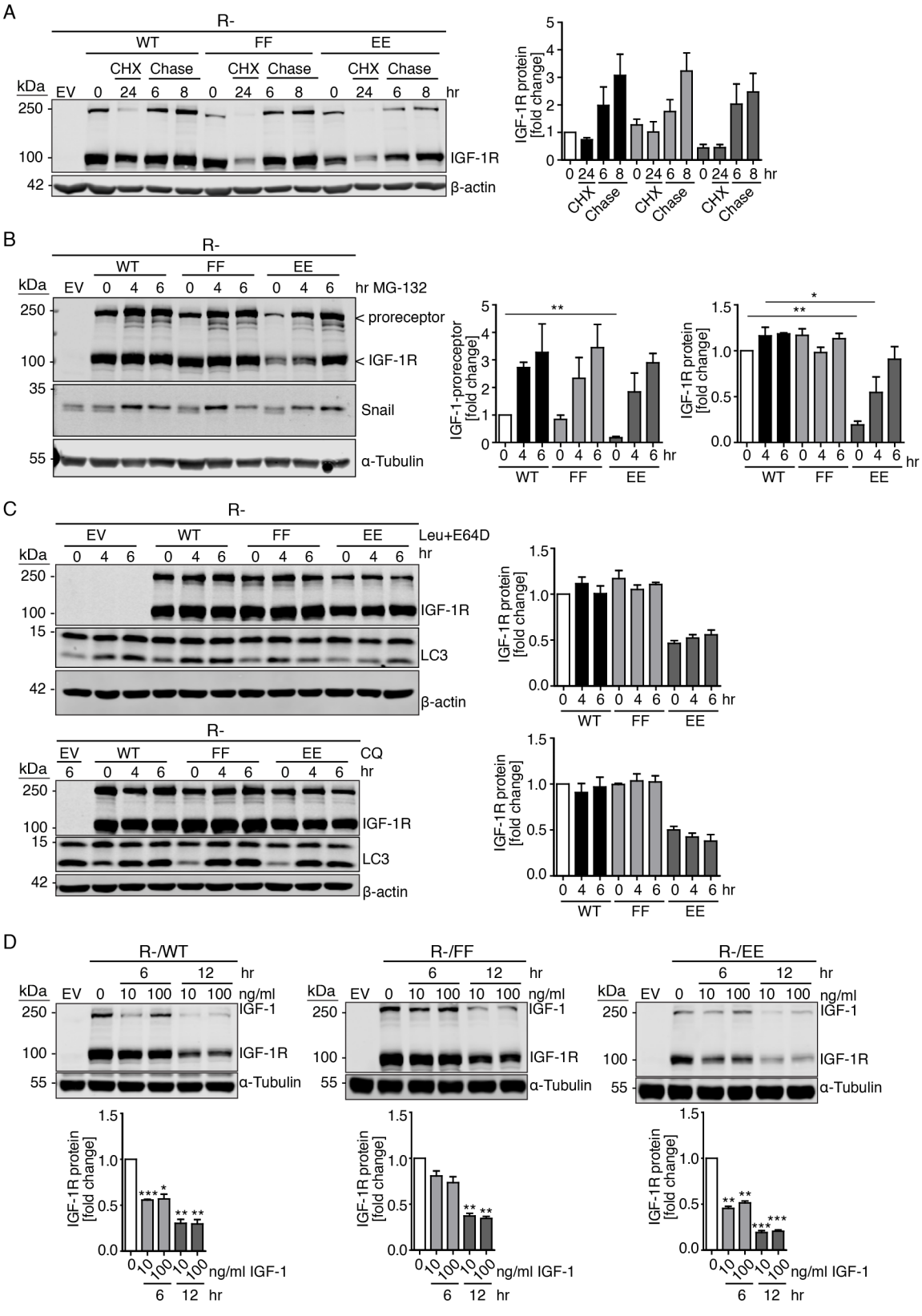
A
R-
WT
FF
EE
CHX
Chase
kDa
EV
0
24
6
8
hr
250
100
42
IGF-1R
β-actin
IGF-1R protein [fold change]
B
MG-132
proreceptor
IGF-1R
35
55
Snail
α-Tubulin
IGF-1-proreceptor [fold change]
C
Leu+E64D
CQ
LC3
15
D
R-/WT
R-/FF
R-/EE
ng/ml
IGF-1
α-Tubulin
ng/ml IGF-1

Fig. 4. The IGF-1R EE mutant is degraded more rapidly than WT IGF-1R. (**A**) Immunoblot for IGF-1R from R- cells transiently expressing IGF-1R WT, FF, or EE cultured in control medium (0 hr) or medium with Cycloheximide (CHX) for 24 hr followed by culture in complete medium (chase). Densitometry quantification is presented as the average fold-change ± SEM in IGF-1R protein relative to the control condition. n=3 independent experiments. Significance was calculated using one-way ANOVA. (**B**) Immunoblot for total IGF-1R and SNAIL from R- cells transiently expressing IGF-1R WT, FF, or EE cultured in control medium (0 hr) or medium containing the proteasome inhibitor MG-132. (**C**) Immunoblots for total IGF-1R and LC3 from R- cells transiently expressing IGF-1R WT, FF, or EE cultured in control medium (0 hr), or medium containing the lysosome inhibitors Leupeptin and E64D (Leu+E64D) or Chloroquine (CQ). **(D)** Immunoblots for IGF-1R from R- cells transiently expressing IGF-1R WT, FF, or EE stimulated with the indicated concentrations of IGF-1 for the indicated times. For (B), (C), (D) densitometry quantification is presented as average fold-change ± SEM in IGF-1R protein relative to control condition. n=3 independent experiments. Significance was calculated using a two-sided one-sample or two-sample *T*-test. *P*-values, *<0.05, **<0.01, ***<0.001.

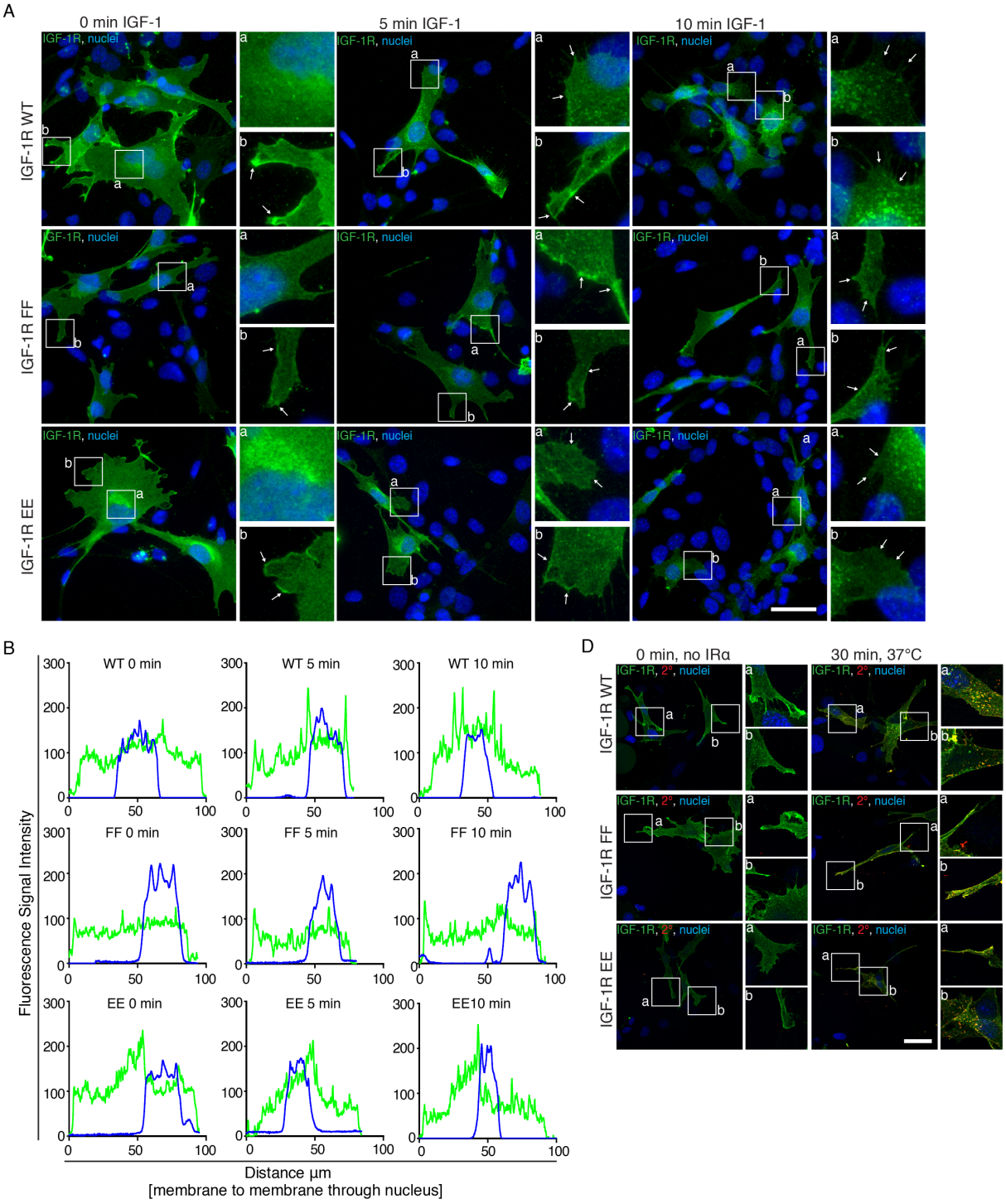
A
0 min IGF-1
5 min IGF-1
10 min IGF-1
IGF-1R WT
IGF-1R FF
IGF-1R EE
IGF-1R, nuclei
B
WT 0 min
WT 5 min
WT 10 min
FF 0 min
FF 5 min
FF 10 min
EE 0 min
EE 5 min
EE10 min
Fluorescence Signal Intensity
Distance µm
[membrane to membrane through nucleus]
C
Surface IGF-1R
[fold change]
10 ng/ml
IGF-1
[min]
TR
SR
WT
FF
EE
D
0 min, no IRα
30 min, 37°C
IGF-1R, 2°, nuclei

Fig. 5. Tyr$^{1250/1251}$ phosphorylation promotes IGF-1R translocation to Golgi.

(**A**) Immunofluorescence of R- cells transiently expressing the IGF-1R WT, FF, or EE mutant showing IGF-1R (green) and nuclei (blue) following serum starvation (0 min) or IGF-1 stimulation (5 and 10 min). Images are representative of n≥4 experiments. (**B**) IGF-1R staining intensity (green) in relation to the nuclear area (blue) measured using the RGB profiler from Image J software along a line drawn through the cell passing through the nucleus. (**C**) Results of in-cell-western from R- cells transiently transfected with WT, FF, or EE IGF-1R probed for total (TR) and surface (SR) IGF-1R. Densitometry quantification is presented as average fold- change ± SEM in IGF-1R surface protein relative to the control condition. n=3 independent experiments. Significance was calculated using a two-sided one-sample or two-sample *T*-test. (**D**) Confocal microscopy showing R- cells transiently expressing the WT, FF, or EE IGF-1R that were serum-starved for 4 hr or incubated with an antibody binding to the IGF-1R α-chain (IRα). Co-localization of IGF-1R IRα antibody [detected with secondary (2°) antibody, in red] and IGF-1Rβ (green) is indicated as a yellow signal. Images are representative of n=2 independent experiments, each with n≥3 cells. *P*-values, *<0.05, **<0.01, ***<0.001. Scale bars, 50 μm.

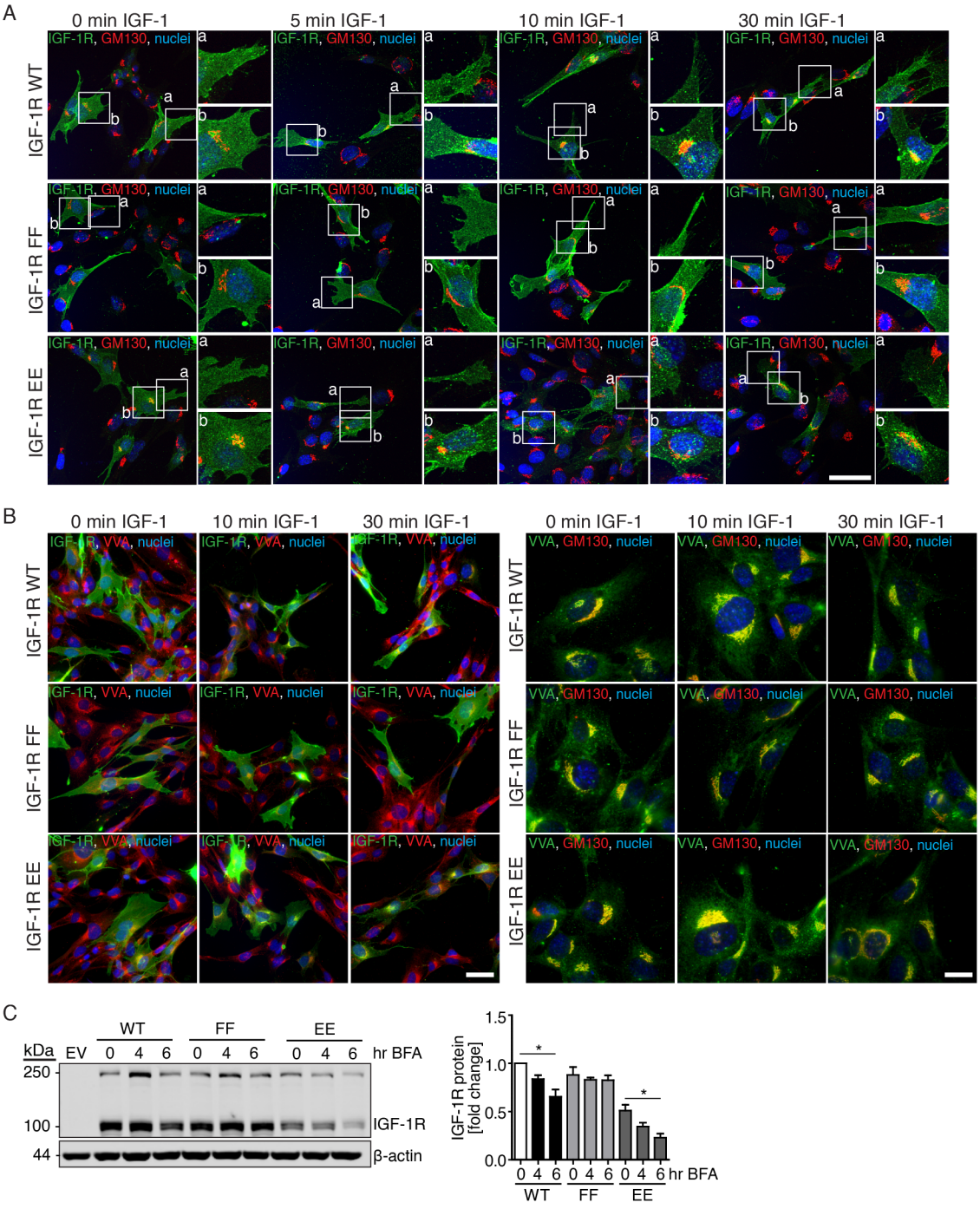

Fig. 6. Tyr$^{1250/1251}$ phosphorylation promotes IGF-1R translocation to the Golgi apparatus.

(**A**) Immunofluorescence of R- cells expressing WT, FF, or EE IGF-1R that were either serum-starved (0 min) or stimulated with IGF-1 (5, 10, 30 min) showing IGF-1R (green), the *cis*-Golgi marker GM130 (red), and nuclei (blue). Scale bar, 50 µm. Images are representatives of n≥3

independent experiments. (**B**) Immunofluorescence of R- cells expressing WT, FF, or EE IGF-1R following IGF-1 stimulation for the indicated times showing IGF-1R (green), the Golgi marker VVA (red or green) or GM130 (red), and nuclei (blue). Representative images of n=2 independent experiments, with n≥3 images acquired for each experiment, are shown. Scale bar, 50 μm scale bar (IGF-1R, VVA) and 20 μm (VVA/GM130). (**C**) Immunoblot for total IGF-1R from R- cells transiently expressing WT, FF, or EE IGF-1R cultured in control medium (0 hr) or medium containing the Golgi disruptor Brefeldin A (BFA). Densitometry quantification is presented as average fold- change ± SEM in IGF-1R protein relative to the control condition. n=3 independent experiments. Significance was calculated using a two-sided one-sample or two-sample *T*-test. *P*-values, *<0.05, **<0.01, ***<0.001.

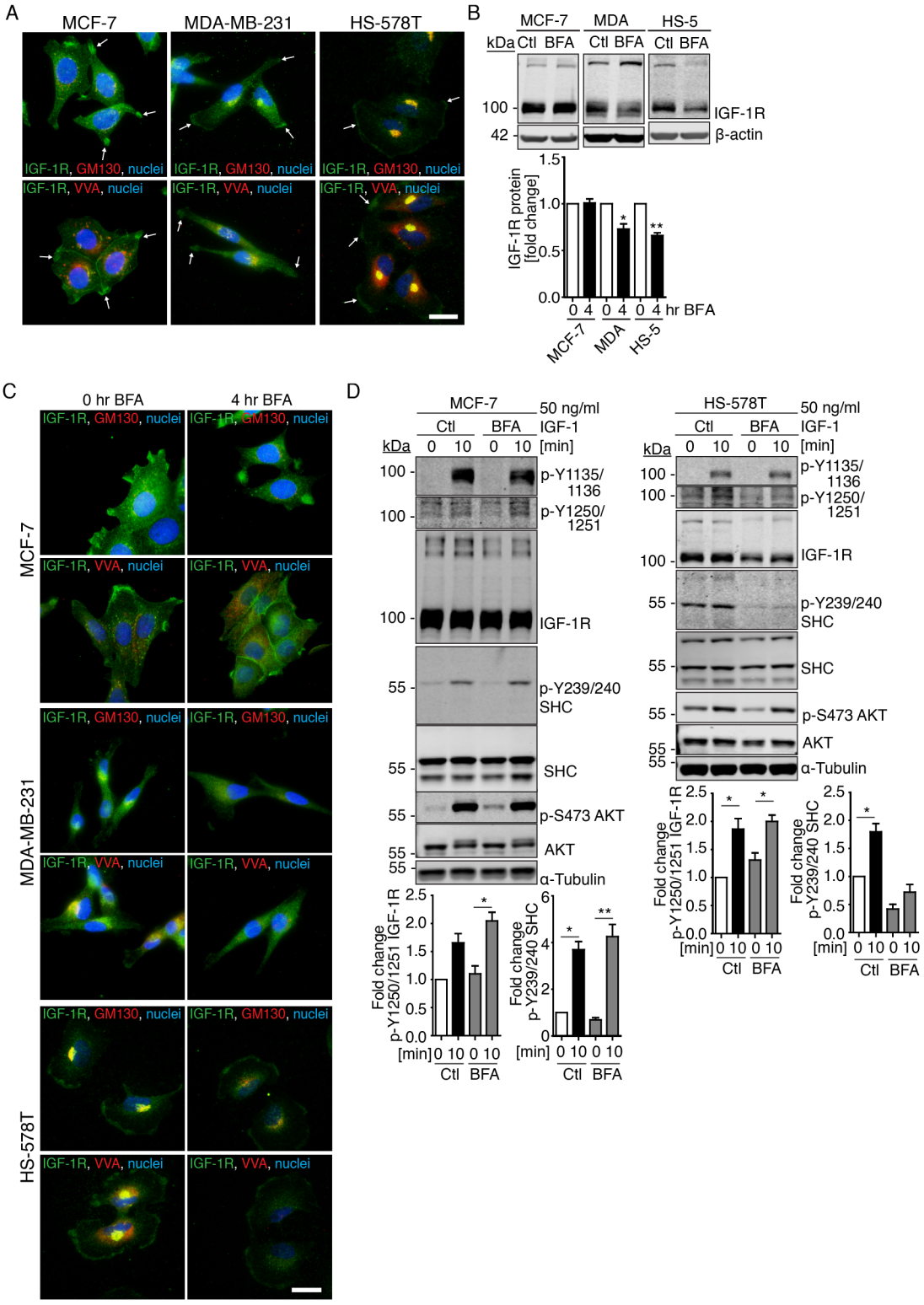

Fig. 7. Tyr$^{1250/1251}$ is phosphorylated in Golgi-localized IGF-1R in migratory cancer cells.

(**A**) Immunofluorescence of MCF-7, MDA-MB-231, and HS578T cells stained to show IGF-1R

(green) and either the *cis*-Golgi marker GM130 or the *cis*/*trans*-Golgi marker VVA (red). Images are representative of n≥3 independent experiments. (**B**) Immunoblot for IGF-1R from MCF-7, MDA-MB-231, and HS-578T cells cultured in control medium (0 hr) or medium containing the Golgi disruptor Brefeldin A (BFA) for 4 hr. Densitometry quantification is presented as average fold-change ± SEM in IGF-1R protein relative to the control condition. n≥3 independent experiments. Significance was calculated using a two-sided one-sample *T*-test.
(**C**) Immunofluorescence of MCF-7, MDA-MB-231, and HS-578T cells cultured in control medium (0 hr) or medium containing Brefeldin A (BFA) for 4 hr and stained for IGF-1R (green) and either GM130 or VVA (red). Images are representatives of n≥3 independent experiments.
(**D**) Immunoblot of the indicated phosphorylated forms of IGF- 1R, SHC, and AKT and total IGR-1R, AKT, and SHC in lysates from MCF-7 and HS-578T cells stimulated with IGF-1 for the indicated time following 4 hr serum starvation in the presence or absence (Ctl) of BFA. Densitometry quantification is presented as the average fold-change ± SEM in ratio of phosphorylated/total protein relative to the control condition. n≥3 independent experiments. Significance was calculated using a two-sided one-sample or two-sample *T*-test. *P*-values, *<0.05, **<0.01, ***<0.001. All scale bars, 20 μm.

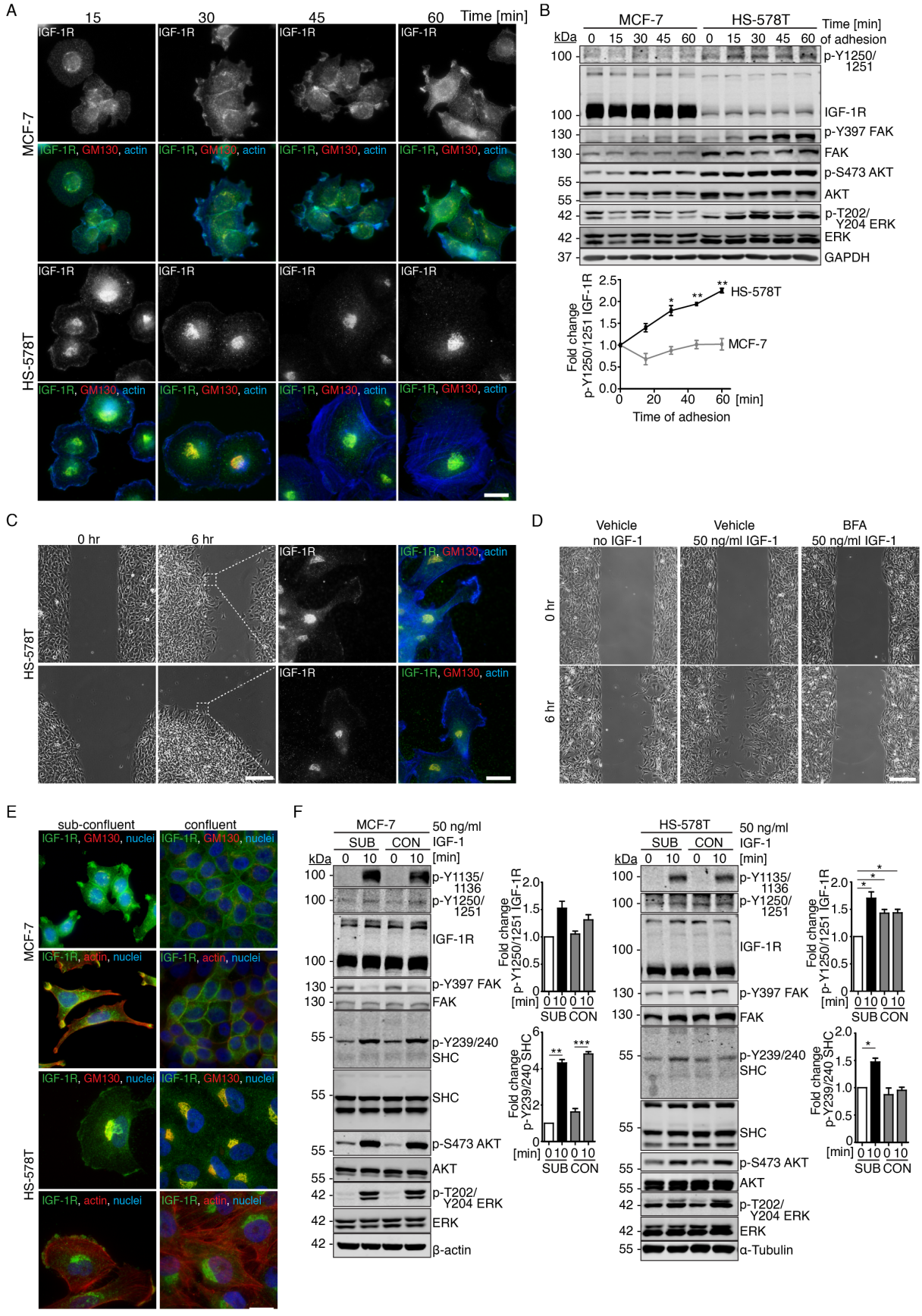
A
15
30
45
60
Time [min]
MCF-7
HS-578T
IGF-1R
IGF-1R, GM130, actin
B
MCF-7
HS-578T
Time [min] of adhesion
kDa
0 15 30 45 60 0 15 30 45 60
100
p-Y1250/1251
100
IGF-1R
130
p-Y397 FAK
130
FAK
55
p-S473 AKT
55
AKT
42
p-T202/Y204 ERK
42
ERK
37
GAPDH
Fold change p-Y1250/1251 IGF-1R
HS-578T
MCF-7
Time of adhesion
[min]
C
0 hr
6 hr
HS-578T
IGF-1R
IGF-1R, GM130, actin
D
Vehicle no IGF-1
Vehicle 50 ng/ml IGF-1
BFA 50 ng/ml IGF-1
0 hr
6 hr
E
sub-confluent
confluent
MCF-7
HS-578T
IGF-1R, GM130, nuclei
IGF-1R, actin, nuclei
IGF-1R, GM130, actin, nuclei
F
MCF-7
HS-578T
50 ng/ml IGF-1
SUB
CON
kDa
[min]
0 10 0 10
100
p-Y1135/1136
100
p-Y1250/1251
IGF-1R
130
p-Y397 FAK
130
FAK
55
p-Y239/240 SHC
55
SHC
55
p-S473 AKT
55
AKT
42
p-T202/Y204 ERK
42
ERK
42
β-actin
55
α-Tubulin
Fold change p-Y1250/1251 IGF-1R
Fold change p-Y239/240 SHC
SUB CON

Fig. 8. Tyr$^{1250/1251}$ phosphorylation correlates with IGF-1R presence in the Golgi in migrating cancer cells. (**A**) Immunofluorescence of MCF-7 and HS-578T cells stained for IGF-1R (green), the cis-Golgi marker GM-130 (red), and actin (blue) at the indicated times after being cultured on Fibronectin-coated coverslips. Images are representative of n≥3 independent experiments. (**B**) Immunoblotting for the indicated phosphorylated forms of IGF- 1R, FAK, AKT, and ERK and total IGF-1R, FAK, AKT, and ERK from MCF-7 and HS-578T cells cultured on fibronectin-coated plates for the indicated times. Densitometry quantification is presented as the average fold-change ± SEM in ratio of phosphorylated/total IGF-1R relative to the control condition over time. n≥3 independent experiments. Significance was calculated using a two-sided one-sample *T*-test. (**C**) Phase-contrast images of HS-578T cells in a scratch wound assay at the indicated time points, and these cells fixed and stained for IGF-1R (green), GM-130 (red), and actin (blue). Images are representative of n=3 independent experiments. (**D**) Phase contrast images of HS-578T cells in a wounding assay in serum-free control medium (no IGF-1) or in the presence of IGF-1, with vehicle or BFA added at 0 and 6 hr after wounding. Images are representative of n=3 independent experiments. (**E**) Immunofluorescence of sub-confluent and confluent MCF-7 and HS-578T cells stained for IGF-1R (green) and either GM130 or actin (red). Images are representative of n=3 independent experiments. (**F**) Immunoblotting for the indicated phosphorylated forms of IGF-1R, FAK, SHC, AKT, and ERK and total IGF-1R, FAK, SHC, AKT, and ERK from sub-confluent (SUB) and confluent (CON) MCF-7 and HS-578T cells stimulated with IGF-1 following serum starvation. Densitometry quantification is presented as the average fold-change ± SEM in ratio of phosphorylated/total protein relative to the control condition. n=3 independent experiments. Significance was calculated using a two-sided one-

sample or two sample *T*-test. *P*-values, *<0.05, **<0.01, ***<0.001. Scale bars, 250 μm (phase) and 20 μm (fluorescence).

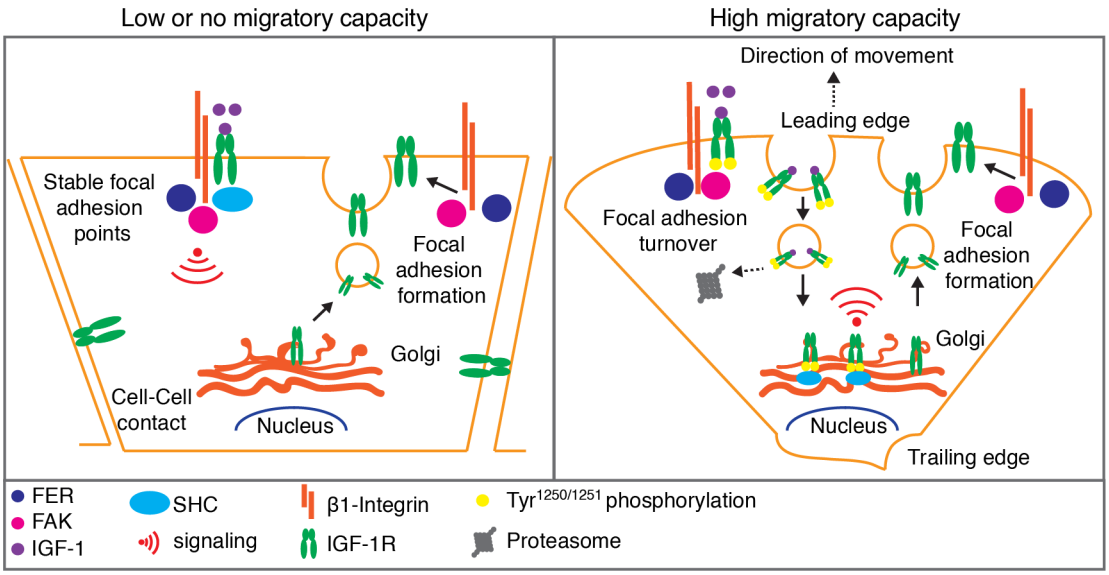

Fig. 9. Model for function of Tyr$^{1250/1251}$ phosphorylation in determining IGF-1R location and signaling in the Golgi apparatus. IGF-1 and adhesion signals promote the phosphorylation of IGF-1R at Tyr$^{1250/1251}$ in both non-migratory and migratory cells. In non-migratory cells, the IGF-1R is predominantly located at the plasma membrane or at stable focal adhesion points. In migratory cells, the IGF-1R is predominantly located in the Golgi apparatus. Upon induction of cell migration, IGF-1R translocates from the Golgi to the leading edge of the cell, subsequently becomes phosphorylated, and returns to the Golgi, where it mediates signaling to downstream effectors, including SHC and ERK.